Towards improved turbulence estimation with Doppler wind lidar VAD scans

Norman Wildmann[1], Eileen Päschke[2], Anke Roiger[1], and Christian Mallaun[3]

[1]Deutsches Zentrum für Luft- und Raumfahrt e.V., Institut für Physik der Atmosphäre, Oberpfaffenhofen, Germany
[2]DWD, Meteorologisches Observatorium Lindenberg - Richard-Aßmann-Observatorium, Lindenberg, Germany
[3]Deutsches Zentrum für Luft- und Raumfahrt e.V., Flugexperimente, Oberpfaffenhofen, Germany

Correspondence: Norman Wildmann (norman.wildmann@dlr.de)

1 Review response

We want to thank the two anonymous reviewers for their valuable feedback and valid points of criticism to our manuscript.

1.1 Review Comment 1

1.1.1 RC1, General Comments

1. *Through the comparison with sonics they are able to show a slight improvement when pulse averaging effects are considered (Fig 6). The main novelty here seems to be the advection correction, which they claim improves the retrievals, but the results are a bit underwhelming (see Fig. 6 and 7). I'm not at all convinced that the tiny improvements in the metrics (bias and correlation) are significant. I would be more inclined to conclude that the advection correction doesn't have a significant effect.*

   The novelty of the paper is not only the advection correction. We re-evaluate a method introduced by Smalikho et al. and validate it in two different campaigns. The analysis method has been modified in ways that are relevant for practical implementation (smaller number of scans, VAD at higher elevation angle) and it was shown that these modifications are legit. The paper describes the first comparison of in-situ aircraft data with lidar turbulence retrievals above 800 m. We show that more validation of this kind will be necessary in future because lidar measurements in low turbulence regimes can significantly underestimate TKE and especially its dissipation rate.

   The advection correction has only a small effect for low elevation VAD scans, which is a positive result as it shows that the Smalikho-method can be used with less restrictive advection filters, if the respective uncertainties are acceptable. Nevertheless, we do show an improvement of the TKE error which increases with higher wind speeds (Figure 8) especially at the 50-m level if the correction is applied. Even more importantly, the advection correction is highly effective if higher elevation VAD scans (here: 75°) are performed to retrieve TKE dissipation rate as is shown in Figs. 9 and 10.

1.1.2 RC1, Specific Comments

1. *Abstract: The first 3 or 4 sentences could be probably be reduced to a single sentence in favor of allowing for a more quantitative summary later in the abstract. As it stands, the abstract lacks sufficient substance. The author should incorporate more hard results from the comparisons with sonic anemometers.*

   We believe that we need to explain the basic idea of the measurements with the introductory sentences even in the abstract but can still add more substance to it in the end. A modified version is given in the revised manuscript.

2. *page 4 line 3: Not everyone will know where Upper Silesia is (including myself until I looked it up), I suggest "... were installed in Upper Silesia, in southern Poland (or where ever), ... "*

   We will add the country Poland in parantheses, the exact location is indicated on a map of Europe in Figure 2.

3. *page 4 line 15: change "... and were finally fixed... " to "... and were finally choosen... "*

   Ok.

4. *Table 1. The Stream Line wavelength is 1.548 μm.*

   From the lidar manufacturer Halo Photonics, we were only provided with the official value of 1.5 μm. If the reviewer can give us a reference for the value he suggests, we will very much like to correct it in the table. On the other hand, this value is not very important for the study and if serious doubts about this value persist, we would rather not mention it at all.

5. *Section 3.2: The author should include the equation for the measured azimuth structure function – since this is key for the dissipation rate retrieval methods.*

   We will include the equation just before Eq. 8 in the revised manuscript:

$$D_L(\psi_l) = \langle [v_r(\theta) - v_r(\theta + \psi_l)]^2 \rangle \tag{1}$$

$$D_a(\psi_l) = D_L(\psi_l) - 2\sigma_e^2 \tag{2}$$

6. *Equation 3: The condition that $\varphi = 35.3°$ should be made more explicit to prevent possible misused.*

   The sentence introducing Equation 3 explicitly states that it is for the special case of $\varphi = 35.3°$.

   We add the suggested addition to the equation.

7. *Page 6, lines 4-6: The author states that the "TKE dissipation rate is estimated through a fit of the measured second-order structure function of horizontal velocity to the theoretical ... " This statement implies that the observations are adjusted to fit the model, when in fact it's the other way around, i.e. the model parameters are adjusted in order to fit the observations. Please rephrase.*

   We apologize for the mistake in language and correct it in the revised manuscript.

8. *Page 6, lines 23-24: Similar to last comment. The author states that "A fit of the azimuth structure to the equation ... " again implies that the observations are being adjusted to fit the model, when in fact it's the other way around. Please*

rephrase.

We apologize for the mistake in language and correct it in the revised manuscript.

9. *Page7, line 1: The author states that "Scanning with Doppler lidar in a VAD implies a volume averaging of radial velocities in longitudinal and transverse directions." Aside from the grammatical errors, this statement is not generally true because transverse averaging is not an issue for step-stair scans, only for continuous motion scans. The author should briefly mention the two different types of scans in their introduction. Also, the author should define what they mean by longitudinal and transverse (i.e. along the beam, and orthogonal to the beam).*

   Velocity azimuth display (VAD) is a term from radar technology where continuous motions of the azimuth motor are the standard. Step-and-stare scans like Doppler-Beam-Swinging techniques are not considered in this manuscript. In any case, even step-and-stare scans with pulsed DWL have a transverse averaging effect due to the pulse-averaging over a certain accumulation time. We add to the manuscript that transverse averaging is regarded for scans with a continuous motion. We also define longitudinal and transverse in the revised manuscript.

10. *Page 7 line 5: change "... radial wind speed..." to "...radial velocity...". Wind speed is a (positive) scalar, velocity is a vector. In this sentence your talking about the radial component of the velocity vector. "Radial wind speed" makes no sense.*

    We change the wording in the revised manuscript.

11. *Page 7 starting at line 7: The discussion here is a bit disjointed and difficult to follow. Equations 5-7 should be listed after the sentence on line 5 (starting with "It is based on the decomposition..."). As it is, these equations are introduced without any corresponding text. One suggestion might be:*
    "In Smalikho and Banakh (2017), this method has been combined with the E89-method to yield TKE, and the momentum fluxes. It is based on the decomposition of radial velocity variance into its subcomponents, i.e.

$$\sigma_L^2 = \sigma_a^2 + \sigma_e^2 \tag{3}$$

$$\sigma_a^2 = \sigma_r^2 - \sigma_t^2 \tag{4}$$

$$\sigma_r^2 = \sigma_L^2 + \sigma_t^2 - \sigma_e^2 \tag{5}$$

where σ_L^2 is the lidar measured variance, σ_a^2 is the lidar measured variance without instrumental error, σ_e^2 is the instrumental error variance, and σ_t^2 is turbulent broadening of the lidar measurement. In Smalikho and Banakh (2017), all of these variances and corresponding structure functions are calculated for single azimuth angles and then averaged."

    We agree that the modifications make the text easier to follow and incorporate the changes in the revised manuscript.

12. *Page 7, line 17: Recommend changing "Substituting σ_e^2 in Eq. 7 with Eq. 8 yields:" to "Combining Eq. 7 with Eq. 8 yields:"*

    We change the sentence in the revised manuscript according to the suggestion of the referee.

13. *Page 7, lines 18-23, including equations 9, 10 and 11: There is a dependence on the separation distance on the right side of equation 9 that presumably cancels such that the right side is effectively constant, i.e. independent of separation distance. This is a subtle point that is not made by the author. Also, in equation 10, the author has substituted Ψ_l with Ψ_1 without any explanation or justification. Please explain.*

We agree that an explanation is lacking here. Since the instrumental error σ_e^2 is assumed to be a constant offset of azimuth structure function $D_a(\psi_l)$ and the lidar measurement $D_L(\psi_l)$, l can actually be chosen arbitrarily in the TKE equation. It is set to $l = 1$ because potential random errors like unstationary flow will be least effective for small separation angles.

14. *Page 8, line 10-11: The author states "...from VAD scans with other elevation angles as well." You should be a bit more specific here, since readers may not know what you mean by "other elevation angles." I assume you're referring to elevation angles different from 35.3°.*

We change the sentence to explicitly say "elevation angles different from 35.3°.

15. *Page 8, line 13-15: The author states "The value of l = 9 is chosen following the example of Smalikho and Banakh (2017) and corresponds to $l\Delta\theta = 9°$ as it was found to be suitable in all conditions in that study." The discussion up to this point had been fairly general. Now, suddenly the author is referring to a very specific VAD scan. The author should be a bit more specific as to which scan (and which experiment) they are referring to.*

Here we define the upper separation angle that will be used in the further manuscript and in all experiments. The separation angle is not referring to a specific VAD scan and in our opinion can be introduced here. We rephrase in the revised manuscript to state that this separation angle was found by Smalikho and Banakh (2017) to be a reasonable value in the ABL. It is illustrated by an example structure function in Figure 3.

16. *Page 8, line 24: change "... radial wind speeds..." to "... radial velocities..."*

All occurences of the term "radial wind speed" are replaced with "radial velocity".

17. *Page 8, line 28: change "... radial wind speeds..." to "... radial velocities..."*

All occurences of the term "radial wind speed" are replaced with "radial velocity".

18. *Page 10, line 1: change "... radial wind speeds..." to "... radial velocities..."*

All occurences of the term "radial wind speed" are replaced with "radial velocity".

19. *Page 10, line 3: change "... radial wind speed..." to "... radial velocitiy..."*

All occurences of the term "radial wind speed" are replaced with "radial velocity".

20. *Page 10, line 6: Recommend changing "Since the mean of the radial wind speed fluctuations vr = 0 by definition, it is:" to something like "Since the mean of the radial velocity fluctuations is zero by definition, equation (20) becomes "*

We change the sentence accordingly.

21. *Page 10 line 5: The author states "(here: g=360 for all azimuth angles)". The reference to a specific value of g here is a bit perplexing. Please explain.*

In this study we work with VAD scans with 1° azimuthal resolution, which yields 360 values per scan. Since we introduce a general method here, we will remove this information at this point of the text.

22. *Equation 20: The summation is over j, but there is no dependence on j in the quantity being summed. Please explain.*
This is a mistake. The summation is over the variable m (index of the azimuth angle within one VAD scan).

23. *Page 10, lines 11-12: change "... radial wind speeds..." to "... radial velocities..."*
All occurences of the term "radial wind speed" are replaced with "radial velocity".

24. *Page 10, line 16-17: The author states "Measured PDFs of the variables ... are fit to the model PDFs to obtain an estimation of the corresponding standard deviations σ_1, σ_2 and σ_3 and probability of bad estimates P_1, P_2 and P_3." This statement implies that the observations are fit to the model. In other words, the observations are tweaked to get agreement with the model. That's certainly not what is happening. Please rephrase.*
We apologize for the confusion in language and rephrase in the revised manuscript.

25. *Section 3.2.2: It seems to me there is some slightly circular logic going on here. From what I gather, your fitting equation 22 to the measured PDFs to obtain estimates of the variance and the false-alarm probability. But since the real distributions aren't Gaussian, you end up computing the variance directly from the data. This begs the question as to why the variance was treated as an adjustable parameter in the first place. Why not just compute the variance from the data to begin with and then use equation 22 to estimate only the false alarm probability. What do the distributions look like? How good (or bad) are the fits?*
A first guess of the standard deviations is needed to find the $\pm 3.5\sigma$ region for the integral over the PDF. All the details of this method are given in Stephan et al. (2018). Since this method is not essential for this study, we do not want to expand too much on it in this manuscript. It is mostly relevant if better measurements in low-signal conditions are targeted.

26. *Section 3.2.3: In this section the author throws down a series of equations without adequate discussion. The authors need to do a better job explaining their line of reasoning.*
We thank the referee for their recommendation on improving the section and incorporate it in the revised manuscript.

27. *Appendix C, lines 17: The author introduces the quantity Xj (i.e. a 1D vector), and then in equation C1 it is indicated to be a 2D matrix, i.e. Xij. Please explain.*
j is the subsample index and i is the index for each element of the subsample. We clarify this in the revised manuscript.

28. *Appendix D: I find no mention of the "FSWF-retrieval" in the paper (did I miss it?). Please elaborate and provide relevant citations.*
Filtered sine-wave fitting is introduced with the corresponding reference in Section 3.2.1, but without giving the abbreviation FSWF. We add this in the revised manuscript.

1.2 Review Comment 2

1.3 RC2, General Comments

1. *The method to retrieve ε from sonic anemometer (and research aircraft) measurements is based on averaging 2 min estimates of ε over 30 min sampling time. Taking the average means that the distribution of ε_{2min} is assumed to be Gaussian, which is not necessarily true as the magnitude of ε_{2min} may vary over several scales of magnitude. When the distribution is not Gaussian, the average will introduce a bias to the ε_{30min} estimate. Therefore, authors should check the shape of the distribution of ε_{2min} values during each 30 min period and choose an estimate for ε_{30min} that is more representative for the distribution of ε_{2min} values, such as the median of these values.*

   We thank the referee for this comment which is very valid and should be considered in the evaluation of sonic anemometer data. An arithmetic mean of dissipation rates ε is not the best solution given the exponential character of the variable. Instead of using the median as suggested, we however believe now that for this study it is more reasonable to calculate the structure function over the full half-hour period and estimate ε from it. Muñoz-Esparza et al. (2018) calculated 2-minute periods because they wanted to see bursts of turbulence on shorter timescales. In our case we are however comparing to lidar measurements that are averaged over half-hour periods, so that a comparison can be best made with the same period for the calculation of the structure function of sonic anemometer data.

   We did investigate the difference between median of 2-minute estimates, mean of 2-minute estimates and 30-minute estimates and can confirm that the referee is right that the 2-minute mean is skewed towards larger values compared to the the median approach. A systematic error can however also occur when the median underestimates the dissipation rate within the half-hour (see Fig. 1). We will not present these results in the revised manuscript because we believe that 30-minute stucture function estimates are the right choice for this analysis.

   In any case, for all possible estimates of ε from sonic anemometers, the differences are small enough to not change the conclusions that are made for the comparison to the lidar retrievals. In Fig. 2 below, we show the differences. The best correlations can be found with the 30-minute structure function estimate. The median estimate shows the highest bias for the S17 method, but the general conclusions remain the same.

1.4 RC2, Specific Comments

1. *It is not obvious to all readers that "DLR Cessna Grand Caravan 208B" is a research aircraft, please, add this to the abstract. Further, it is not clear why do you introduce the research aircraft data in this study as the title is about improvement of turbulence estimation using Doppler wind lidars. For validation purposes research aircraft data cannot be considered as robust as sonic anemometer data. In fact, the explanation for using aircraft measurements is provided only in Section 5 on lines 8-9 of page 21. This explanation should be given already in the abstract but also in the Introduction (Section 1) and maybe also in Section 3.3.*

   We add the term "research aircraft" in the abstract explicitly and also explain that the research aircraft is a unique

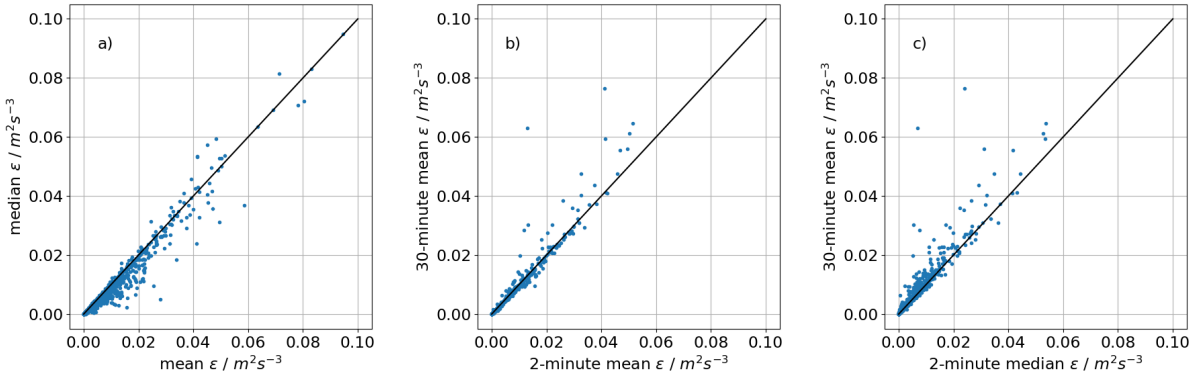

Figure 1. Comparison of different estimations of ε from sonic anemometers: a) mean of 2-minute structure function estimates versus median of 2-minute structure function estimates; b) mean of 2-minute structure function estimates versus 30-minute structure function estimates; c) mean of 2-minute structure function estimates versus 30-minute structure function estimates

possibility to collect in-situ turbulence measurements above the heights that are in reach with sonic anemometers for example.

2. *Section 2, page 2, lines 33-34: "data from two different sites and sets of instruments": This is not clear: you use data from four DWLs (three in Upper Silesia, one at Falkenberg), from two sonic anemometers and from one research aircraft. Although you introduce the measurements in two Figures (Figures 1 and 2), it does not change the fact that you have several type of instruments and sites, not just two of each.*

   We change the text to only state that measurements from two different experiments are analyzed. The details of the sites and the instrumentation is given in detail throughout the section: "In this study, data from two different experiments are analyzed. Both of the experiments and the instrumentation is introduced in this section."

3. *Section 2.1., page 3, line 19: remove "and infrared gas analysers LI7500 (LiCor Inc.)" because you do not use this data.*

   We remove the information about the gas analyzer in the text: "Continuous turbulence measurements (20 Hz sampling frequency) using sonic anemometer of type USA-1 (METEK GmbH) are performed at the 50m and 90m levels of the tower and have been used for validation purposes. The instruments are mounted at the tip of the booms pointing towards South."

4. *Section 2.2, the first two paragraphs on page 4: the description of the CoMet mission is too detailed and not relevant to the topic of this paper, as here the aim is not to investigate CO2 or methane but to develop DWL data processing methods. Please, provide here only such information that is relevant for the present study.*

   We believe that the information about the CoMet campaign is relevant, because it puts the DWL measurement into context for the special issue to which this manuscript has been submitted. This manuscript is important for the CoMet research community, so that we want to make a connection to the overall project.

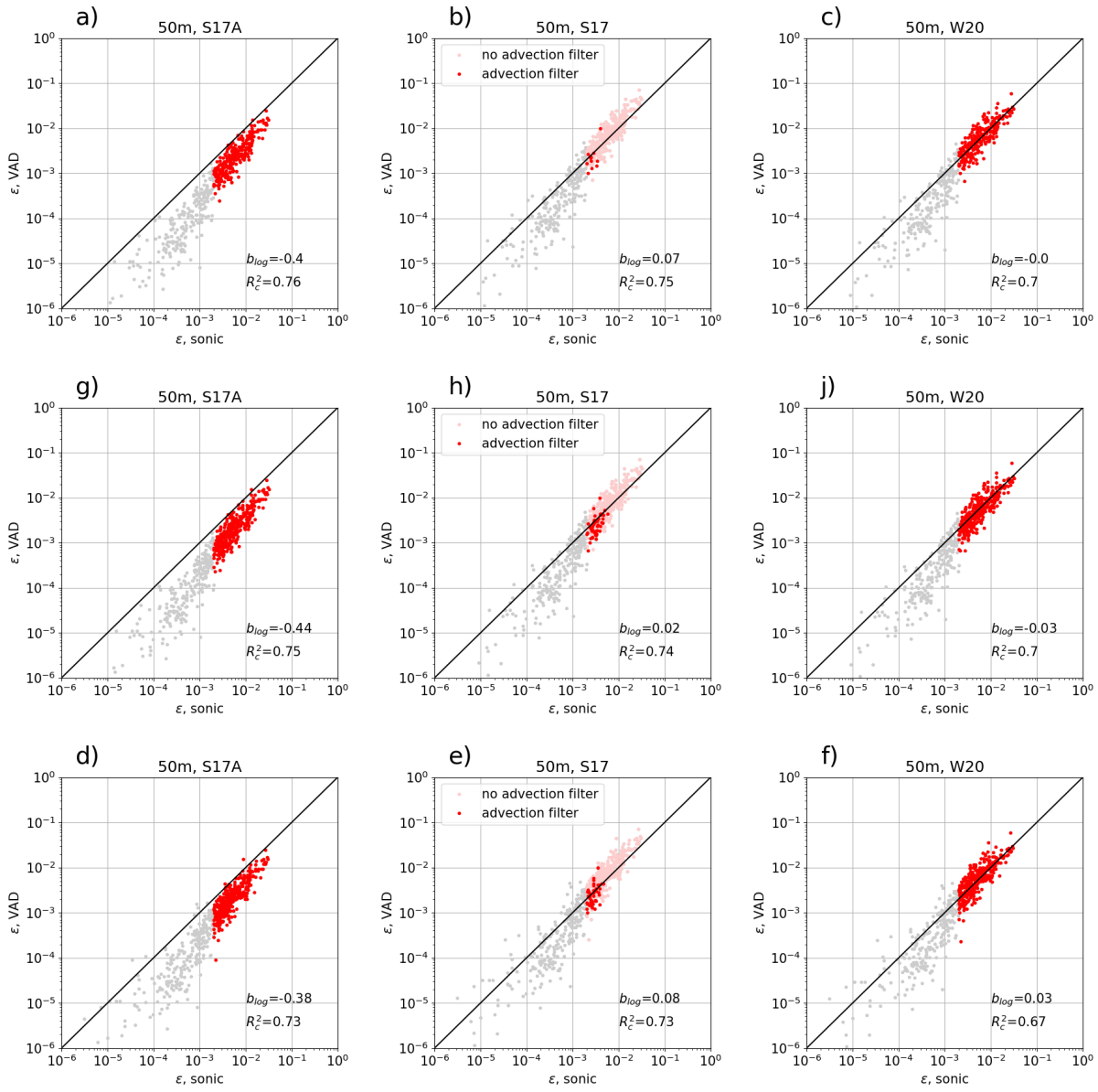

Figure 2. Scatter plot of lidar dissipation rate retrieval against sonic anemometer dissipation rate, calculated with different methods. a)-c) show the 30-minute structure function estimate, d)-f) show the mean of 2-minute structure function estimate (as in the discussion manuscript) and g)-j) show the median of 2-minute structure function estimate.

5. *Page 4, line 19: angle should read 35.5° not 35°.*

   Ok.

6. *Page 4, lines 20-21, 2 comments:*

   (a) *Check the tense of verbs to be consistent.*

   (b) *The acronyms of the Doppler lidars in Upper Silesia region are misleading: for the research aircraft you use the acronym "DLR" (e.g. in the abstract but also on line 8 of page 4) and for Doppler lidars you have introduced the acronym "DWL". Why do you introduce here another acronym for DWL, i.e., "DLR"? Please, use only one acronym for Doppler wind lidars throughout the paper.*

   We change the naming of the lidars in the CoMet campaign to DWL#1-DWL#3 in the revised manuscript. The tense of the verb are all changed to past tense.

7. *Page4, lines 23-25: "a case study on 5 June 2017, on which D-FDLR was performing long straight and level legs between 800 m and 1600 m as indicated in the flight path in Fig. 2." This is the first time you introduce the research aircraft data and it is somewhat vague. Please, provide more information on why did you choose this data set, how did you select this specific period, what kind of instrumentation there was onboard, how accurate are the turbulence measurements from the aircraft in general, etc?*

   More information with the relevant reference is given in this Section in the revised manuscript.

8. *Page 6, line 7: "the values are calculated for 2-minute intervals and then averaged over half-hour periods.". Include here information about the distribution of values calculated for 2-minute intervals, to show that the average is (or is not) a representative parameter for the population of values (see also the major comment).*

   See above answer to major comment.

9. *Page 7, line 19: Should it read Eq.2 instead of Eq.3?*

   It is actually Eq. 3, but the way this is written is confusing and we rephrase in the revised manuscript.

10. *Page 7, line 20: Why does Ψ_l change to Ψ_1 here? Please, explain what it means that l=1?*

    We agree that an explanation is lacking here. Since the instrumental error σ_ϵ^2 is assumed to be a constant offset of azimuth structure function $D_a(\psi_l)$ and the lidar measurement $D_L(\psi_l)$, l can actually be chosen arbitrarily in the TKE equation. It is set to $l = 1$ because potential random errors like unstationary flow will be least effective for small separation angles.

11. *Page 7, line 25: Typo: "Kolmogorov-Obhukov spectrum"*

    ok.

12. *Page 8, Equation (15): It is not clear how this Equation is derived from Eq. 13 and 8: what happens to σ_ϵ^2 that was in Equation 8?*

By taking the difference of $D_a(\psi_l) - D_a(\psi_1)$, σ_e^2 gets eliminated. We rephrase slightly to be clearer: "Using Eq. 13 and 8, ε can be retrieved from $D_a(\psi_l) - D_a(\psi_1)$:"

13. *Page 9, line 8: "In (Smalikho and Banakh, 2017)" change to "In Smalikho and Banakh (2017)"*
    Ok.

14. *Page 10, Equation 20: There is no index j in the equation (which is included in the summation). Moreover, are there some parenthesis missing?*
    The index j is a mistake, it should be m. There are no paranthesis missing.

15. *Page 12, Section 3.3: Again, it is not clear why research aircraft data is used: is it used a) because it gives more reliable results than DWLs and therefore can be used for validation of DWL data or b) is it used because it would be interesting to know how good the research aircraft data is compared to DWLs (and sonics)?*
    We consider turbulence measurements with flow probes on research aircraft a well-established method which provides more reliable measurements than a DWL since it does not depend on many assumptions except the Taylor's hypothesis.

16. *Page 14, Figure 5: It is not possible to see the dotted line in panel (a). Moreover, in the caption, could you provide the Equation numbers for the averaged variance and total variance methods in order to strengthen the link between the theory and the results.*
    Since the lines for the both methods lie almost on top of each other and the dotted line is thus hard to see we include a subplot showing the difference between the two methods for the presented time series (see Fig. 3). The references to the equations are added in the revised manuscript.

17. *Page 14, line 5: "modified version W19 introduced in this study", maybe you should use acronym W20 for the method introduced in this paper?*
    We changed the acronym throughout the manuscript.

18. *Page 15, Figure 6: Does the biases in (b) and (e) include all points or only those after the advection filter?*
    All points except the grey points below the threshold are used. We will clarify in the caption. We think it is important to use all points to evaluate the effect of the advection correction.

19. *Page 17, Figure 8: Why there is an oscillatory pattern in TKE bias as a function of horizontal wind speed? The oscillatory pattern is more significant than the differences between the methods, and therefore it should be discussed. Could you also provide here the amount of data in each bin, maybe by adding another y-axis for that?*
    There is no physical reason for an oscillatory pattern in TKE vs. horizontal wind speed. The shape of the curve is merely a specialty of the dataset where more values of certain bins fall in nighttime hours with lower TKE and thus also lower absolute error in TKE. We add the number of data points in the bin in Figure 8 of the manuscript as shown here in Fig. 4

20. *Page 18, line 9: "Here, it shows that the difference between S17 and W19 only occurs at the very lowest level" - this cannot really be seen from Figure 12.*

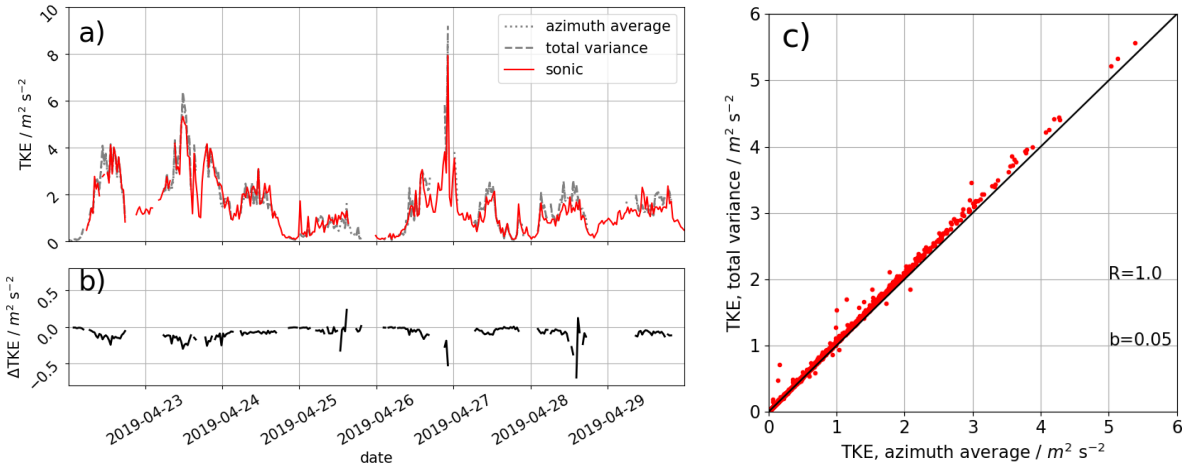

Figure 3. Time series of TKE from lidar retrievals compared to a sonic anemometer at 90 m above ground level (a), the differencec between the lidar retrieval with averaged variances (Eq. **??**) at specific azimuth angles θ to the modified, total variance method (Eq. **??**) (b) and the scatterplot for the whole experimental period (c).

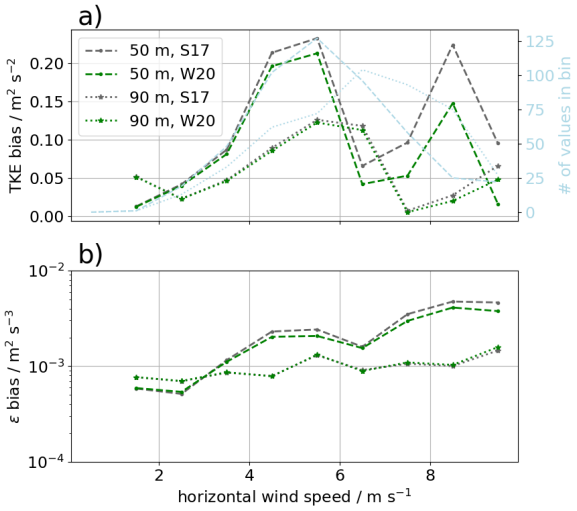

Figure 4. Difference of lidar retrieval of TKE (a) and TKE dissipation rate (b) compared to sonic anemometer as a function of wind speed.

It shows that for DLR1, there is a small difference between the two methods, but it is not very well visible. We change the discussion of this figure in the revised manuscript.

21. *Page 19, Figure 11: Another horizontal axis with a km scale would be nice, because in the text you give the length of the flight path in kilometers.*

    We change the plot to give the x-axis in kilometers instead.

22. *Page 20, Figure 12: Different DWL lines are extremely difficult to see in both panels. Consider using different colors for the lines and rescaling of the figures.*

    We rescaled the figure and changed the color of the greyscale for the S17-method slightly for better readability of the plot.

23. *Page 20, lines 16-18: "The advection effects are most relevant at the lowest measurement heights where the spatial separation of lidar beams along the VAD cone Δy are small." This is true, but what could perhaps be also mentioned is that the advection speed increases with height because of the logarithmic wind profile.*

    We add this thought to the discussion. In our observation, the effect of increasing wind speed with height is however not as strong as the effect of a counteracting larger Δy.

24. *Page 21, lines 1-3: "dissipation rates of values smaller than $10^{-3}m^2s^{-3}$ are underestimated by the lidars, likely because the small scale fluctuations that are carrying much of the energy in these cases, cannot be resolved any more." This can be true, but you should still check the method to retrieve dissipation rates from sonic anemometers as mentioned in the previous comments.*

    As shown above we have evaluated the sonic anemometer retrieval and agree that there can be differences between different methods to obtain a representative value of ε within the half-hour period. However, the strong underestimation of lidar measurements below $10^{-3}\mathrm{m}^2\mathrm{s}^{-3}$ is much more significant and found in any case.

25. *Page 21, lines 8-10: this information should be provided much earlier in the manuscript. This is not just a result but also the motivation to use research aircraft data in the first place.*

    More information on the motivation to use aircraft data is added to Section 2.2. in the revised manuscript.

2 Relevant changes to the manuscript

We list here the relevant changes to the manuscript:

1. Abstract:
   - Text modifications in response to referee comments. More focus on results of the study.
2. Introduction:
   - Text modifications in response to referee comments.
3. Section 2:
   - Text modifications in response to referee comments.
4. Section 3:
   - Text and equation modifications in response to referee comments.
5. Section 4:
   - Text and equation modifications in response to referee comments.
   - Added subplot to Figure 5.
   - Figures 6,7,8 updated with recalculated dissipation rates from sonic anemometers (response to referee comment).
   - Figure 8&10: Added number of data points per bin in the plot.
   - Figure 10: Changed x-axis to km.
   - Figure 12: Changed line colors and scaling.
6. Conclusions:
   - Text modifications in response to referee comments.
7. Appendix:
   - Text modifications in response to referee comments.

References

Stephan, A., Wildmann, N., and Smalikho, I. N.: Spatiotemporal visualization of wind turbulence from measurements by a Windcube 200s lidar in the atmospheric boundary layer, Proc.SPIE, 10833, 10 833 – 10 833 – 10, https://doi.org/10.1117/12.2504468, 2018.

Muñoz-Esparza, D., Sharman, R. D., and Lundquist, J. K.: Turbulence Dissipation Rate in the Atmospheric Boundary Layer: Observations and WRF Mesoscale Modeling during the XPIA Field Campaign, Monthly Weather Review, 146, 351–371, https://doi.org/10.1175/MWR-D-17-0186.1, 2018.

Towards improved turbulence estimation with Doppler wind lidar VAD scans

Norman Wildmann[1], Eileen Päschke[2], Anke Roiger[1], and Christian Mallaun[3]

[1]Deutsches Zentrum für Luft- und Raumfahrt e.V., Institut für Physik der Atmosphäre, Oberpfaffenhofen, Germany
[2]DWD, Meteorologisches Observatorium Lindenberg - Richard-Aßmann-Observatorium, Lindenberg, Germany
[3]Deutsches Zentrum für Luft- und Raumfahrt e.V., Flugexperimente, Oberpfaffenhofen, Germany

Correspondence: Norman Wildmann (norman.wildmann@dlr.de)

Abstract. The retrieval of turbulence parameters with profiling Doppler wind lidars (DWL) is of high interest for boundary-layer meteorology and its applications. The DWL measurements extend beyond the observations with meteorological masts and are comparably flexible in their installation. Velocity-azimuth display (VAD) type scans can be used to retrieve turbulence kinetic energy (TKE) dissipation rate through a fit of measured azimuth structure functions to a theoretical model. At the elevation angle of 35.3° it is also possible to derive TKE. ~~We show~~ Modifications to existing retrieval methods are introduced in this study ~~how modifications to existing methods allow to retrieve TKE and its dissipation rate even with a small~~ to reduce the errors due to advection and enable retrievals with a low number of scans~~, how a simple correction for advection improves the results at low altitudes and that VAD scans at different elevation angles with the same instrument provide comparable results of TKE dissipation rate after all filters and corrections. For this purpose, data~~. Data of two experiments are utilized for validation: First, measurements at the Observatory Lindenberg – Richard-Aßmann Observatory (MOL-RAO) are used for validation of the DWL retrieval with sonic anemometers on a meteorological mast. Second, distributed measurements of three DWL during the CoMet campaign ~~are analyzed and~~ with two different elevation angles are analyzed. For the first time, the DWL VAD turbulence retrievals are compared to in-situ measurements of ~~the~~ a research aircraft (here: DLR Cessna Grand Caravan 208B~~. The comparison to in-situ instruments shows that~~) which allows measurements of turbulence above the altitudes that are in range for sonic anemometers.

From the validation against the sonic anemometers we confirm that lidar measurements can be significantly improved by the introduction of the volume averaging effect into the retrieval. We introduce a correction for advection in the retrieval which only shows minor reductions in the TKE error for 35.3° VAD scans. A significant bias reduction can be achieved with this advection correction for the ~~methods to improve turbulence retrievals from VAD scansintroduced in this study are effective, especially at low altitudes and for narrow cone angles, but it also shows the limits of turbulence measurement with state-of-the-art DWL~~ TKE dissipation rate retrieval from 75° VAD scans at the lowest measurement heights. Successive scans at 35.3° and 75° at the CoMet campaign are shown to provide TKE dissipation rates with a good correlation of $R > 0.8$ if all corrections are applied. The validation against the research aircraft encourages more and targeted validation experiments to better understand and quantify the underestimation of lidar measurements in low turbulence regimes and altitudes above tower heights.

1 Introduction

The observation of turbulence in the atmosphere and in particular the atmospheric boundary layer (ABL) is of great importance for basic research in boundary-layer meteorology as well as in applied fields such as aviation, wind energy (van Kuik et al., 2016; Veers et al., 2019) or pollution dispersion (Holtslag et al., 1986).

A wide range of instruments are used to measure turbulence: sonic anemometers are nowadays the most popular in-situ instrument which can be installed on meteorological masts and provide continuous data of the three-dimensional flow and its turbulent fluctuations (Liu et al., 2001; Beyrich et al., 2006). For in-situ measurements above the height of towers, airborne systems are applied such as manned aircraft (Bange et al., 2002; Mallaun et al., 2015), remotely-piloted aircraft systems (RPAS, van den Kroonenberg et al., 2011; Wildmann et al., 2015) or tethered lifting systems (TLS, Frehlich et al., 2003) which can be equipped with turbulence probes such as multi-hole probes or hot wire anemometers. A different category of instruments are remote-sensing instruments such as radar, sodar and lidar which can measure wind speeds and allow the retrieval of turbulence based on assumptions of the state of the atmosphere and the structure of turbulence. In this study, we focus on ground-based Doppler wind-lidars (DWL), which have become increasingly popular in boundary-layer research because of their ~~light weight~~ease of installation, invisible and eye-safe lasers, their reliability and high availability which is only restricted by clouds/fog and rain or very low aerosol content in the atmosphere.

A variety of methods already exist to retrieve turbulence from DWL measurements. They can be categorized according to the respective scanning strategy applied: the simplest scanning pattern is a constant vertical stare to zenith, which allows to obtain variances of vertical velocity and estimates of turbulence kinetic energy (TKE) dissipation rate (O'Connor et al., 2010; Bodini et al., 2018). More complex are conical scans (velocity azimuth display, VAD) with continuous measurements along the cone (Banakh et al., 1999; Smalikho, 2003; Krishnamurthy et al., 2011; Smalikho and Banakh, 2017). These scans include information on the horizontal wind component as well. A simplification of VAD scans are Doppler-beam-swinging (DBS) methods, that reduce the number of measurements taken along the cone to a minimum of 4-5 beams and thus increase the update rate for single wind profile estimations (Kumer et al., 2016). Both, VAD and DBS are popular scanning strategies that are applied in commercial instruments. Kelberlau and Mann (2019a, b) introduced new methods to obtain better turbulence spectra from conically scanning lidars by corrections for the scanner movement. Significantly different scanning strategies are vertical (or horizontal) scans which can also provide vertical profiles of turbulence (Smalikho et al., 2005), but even allow deriving two-dimensional fields of TKE dissipation rate (Wildmann et al., 2019). Multi-Doppler measurements require more than one lidar with intersecting beams, but do not need assumptions on homogeneity to measure turbulence at the points of the intersection directly (Fuertes et al., 2014; Pauscher et al., 2016; Wildmann et al., 2018). For operational or continuous monitoring of vertical profiles of turbulence in the ABL, VAD or DBS scans are most suitable. At an elevation angle of 35.3°, a VAD scan allows to retrieve TKE, its dissipation rate, integral length scale and momentum fluxes according to a method that was first developed for radar by Kropfli (1986) and adapted for lidar later by Eberhard et al. (1989) using the variance of radial velocities along the scanning cone. Further improvements of this method have been implemented by Smalikho and Banakh (2017) and Stephan et al. (2018), which also account for lidar volume averaging effects. We introduce modifications on the estimation of

structure function and variances in order to be able to retrieve turbulence parameters from a smaller number of VAD scans. For conditions with significant advection, the method ~~is not applicable and causes large~~ can cause errors, especially at low altitudes where the cone diameter of the VAD scan is small. With this study, we propose a method to ~~significantly~~ reduce this error. We also apply the turbulence retrieval to VAD scans with 75° elevation angle, which still allows to retrieve TKE dissipation rate. In this case the advection correction is particularly important. The experiments that were carried out are explained in Sect. 2. The methods and the new developments are explained in Sect.3. A focus of this study is on the validation of the lidar measurements with sonic anemometers and airborne in-situ measurements. The results of the validation are presented in Sect. 4. Conclusions and an outlook are given in Sect. 5.

2 Experiment description

In this study, data from two different ~~sites and sets of instruments~~ experiments are analyzed. Both of the ~~sites~~ experiments and the instrumentation is introduced in this ~~Section~~section.

2.1 The MOL-RAO Falkenberg field site

The Meteorological Observatory Lindenberg – Richard-Aßmann Observatory (MOL-RAO) is part of Deutscher Wetterdienst (DWD), the national meteorological service of Germany. The observatory is situated in the East of Germany, approximately 65 km to the South-East of the center of Berlin. MOL-RAO runs a comprehensive operational measurement program to characterize the physical structure and processes in the atmospheric column above Lindenberg. Measurements of ABL processes form an essential part of it, they are carried out at the boundary layer field site (in German: Grenzschichtmessfeld, GM) Falkenberg, about 5 km to the South of the main observatory site. The GM Falkenberg is situated in a rural landscape dominated by forest, grassland and agricultural fields (see Fig. 1). A central measurement facility at the Falkenberg site is a 99m tower, equipped with booms to carry sensors every 10 m.

Since 2014, MOL-RAO is using a DWL „Stream Line“ (Halo Photonics Ltd.) for boundary layer measurements. From that time the device has been extensively tested with respect to its operational use for wind and turbulence measurements. This included, for instance, tests on the technical robustness and data availability under all weather conditions, but also tests of different scanning strategies and retrieval methods for the 3D wind vector and for the TKE. The position of the DWL during a measurement period from 2 April 2019 through 30 April 2019 was at the western edge of the field site, at about 500 m distance from the 99m tower. It should be noted that there is a small patch of forest about 300 m to the W-NW of the lidar site. During this period the system continuously performed VAD scans with an elevation angle of ~~35~~35.3° elevation which will be analysed for turbulence retrievals in this study.

Continuous turbulence measurements (20 Hz sampling frequency) using ~~the eddy-covariance method with sonic anemometer-thermometer~~ sonic anemometer of type USA-1 (METEK GmbH) ~~and infrared gas analysers LI7500 (LiCor Inc.)~~ are performed at the 50m and 90m levels of the tower and have been used for validation purposes. The instruments are mounted at the tip of the booms pointing towards South~~with the LI7500 behind the USA-1~~.

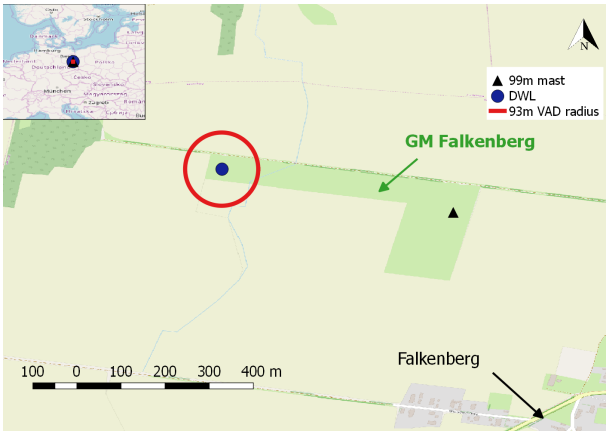

Figure 1. Sketch of the measurement site at MOL-RAO, GM Falkenberg. Map data ©OpenStreetMap contributors 2019. Distributed under a Creative Commons BY-SA License.

2.2 The CoMet (CO_2 and Methane) Mission 2018

Within the scope of the CO_2 and Methane Mission (CoMet) that was conducted in spring 2018, three Doppler wind lidars of type Leosphere Windcube 200S (details see Tab. 1) were installed in Upper Silesia (Poland) with the purpose of providing spatially distributed wind and turbulence measurements in the ABL. CoMet aims at a better understanding of the budgets of the two most important anthropogenic greenhouse gases (GHGs), CO_2 and CH_4. For this purpose, the research aircraft HALO (high altitude and long range) was taking remote sensing and in-situ measurements over large parts of the European continent. A dedicated area of high interest was the region of Upper Silesia, where large amounts of methane are known to be released due to the intensive coal extraction activities in the respective Coal Basin. During the CoMet campaign, the DLR Cessna Grand Caravan 208B (D-FDLR) aircraft was equipped with in-situ instruments to measure greenhouse gases as well as thermodynamic variables.

The DWL measurements are particularly helpful to support the CoMet measurements by providing wind information which is essential to derive emission flux estimates from passive remote sensing (Luther et al., 2019) or in-situ measurements of mass concentrations (Fiehn et al., 2020). The DWL wind information can also be used to validate modeled wind of the transport models for greenhouse gases. The lidars were remotely operated during the whole CoMet campaign period from 16 May 2017 to 17 June 2017 and were continuously measuring. The locations of the three lidars were planned to cover the whole region of interest and were finally ~~fixed~~ chosen based on logistical constraints.

The lidars were operating in VAD modes with two different elevation angles. Since the focus for the CoMet campaign was on continuous wind profiling and a good height coverage was desired, the lidars were programmed to perform VADs with an elevation angle of 75° (see Tab. 1, VAD75) for a longer period, i.e. 24 scans (≈29 minutes), followed by only six scans (≈7 minutes) at ~~35~~35.3° elevation (VAD35) for turbulence retrievals.

As shown in Fig. 2, the three lidars were separated by several tens of kilometers and ~~are~~ were located in different terrain

types. While ~~DLR~~DWL#1 ~~is~~ was in a mixed rural and urban area, ~~DLR~~DWL#2 ~~is~~ was in a mostly forested environment and ~~DLR~~DWL#3 ~~is~~ was in close vicinity to the lake Goczalkowicki. The main wind direction during the campaign was from the East, with particularly strong winds during nighttime low-level jet (LLJ) events. In this study we analyze statistics of the whole campaign, as well as a case study on 5 June 2017, on which D-FDLR was performing long straight and level legs between 800 m and 1600 m as indicated in the flight path in Fig. 2. Since the D-FDLR was focusing on GHG measurements at the hotspots of the Upper Silesian Coal Basin, there are no more straight and level flight paths that allow for turbulence retrieval. On this day however, the research aircraft provides a unique possibility to validate lidar measurements with in-situ measurements at higher altitudes that cannot be reached with sonic anemometers. The flow probe and inertial measurement unit on the D-FDLR are well-established instruments that allow reliable measurements of the 3D-wind vector and turbulence (Mallaun et al., 2015).

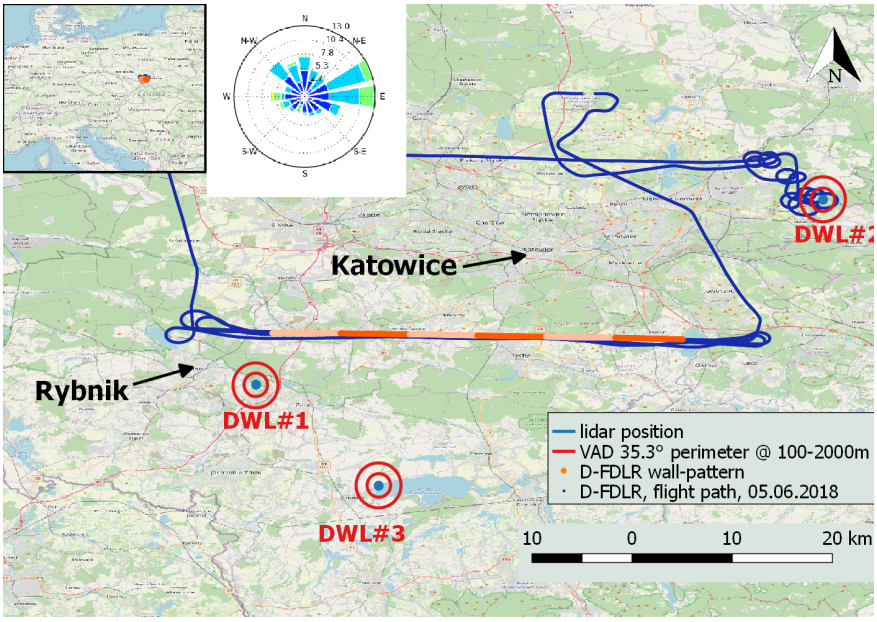

Figure 2. Sketch of the measurement site in Upper Silesia. Red circles show the extent of the VAD-scan at 35.3° for 100 m and 2000 m at the respective lidar location. The orange line marks the flight path of D-FDLR on 5 June 2017. The different shades of orange are used to indicate a subdivision of the flight leg in shorter sublegs. Map data ©OpenStreetMap contributors 2019. Distributed under a Creative Commons BY-SA License.

Table 1. Main technical specifications of the Doppler wind lidars.

	Windcube 200S, VAD75	Windcube 200S, VAD35	Stream Line
Wavelength λ	1.54 µm	1.54 µm	1.5 µm
Pulse length τ_p	200 ns	200 ns	180 ns
Time window T_w	288 ns	144 ns	240 ns
Bandwidth	26.7 m s^{-1}	26.7 m s^{-1}	19.4 m s^{-1}
Elevation angle φ	75°	35.3°	35.3°
Angular speed	5°s^{-1}	5°s^{-1}	5°s^{-1}
Pulse repetition frequency	20 kHz	20 kHz	15 kHz
Accumulation time	200 ms	200 ms	133 ms
CNR filter	-20..0 dB	-20..0 dB	-15..0 dB

3 Methods

3.1 Sonic anemometer turbulence measurements

From the sonic anemometers on the meteorological mast, TKE and TKE dissipation rate are calculated. TKE is calculated from the sum of variances $E_{\mathrm{TKE}} = 0.5\left(\sigma_u^2 + \sigma_v^2 + \sigma_w^2\right)$. TKE dissipation rate ε is estimated through a fit of the ~~measured second-order structure function of horizontal velocity to the theoretical,~~ theory of the longitudinal Kolmogorov-structure function in the range $\tau_1 = 0.1$ s to $\tau_2 = 2$ s ~~. As in Muñoz-Esparza et al. (2018) , who~~ to the measured second-order structure function of horizontal velocity. Muñoz-Esparza et al. (2018) showed that the structure function method is more robust than estimates from spectra~~, the values~~ . For this study, in order to have the best possible comparison to the lidar measurements the values for ε are calculated for ~~2-minute intervalsand then averaged over half-hour periods~~30-minute intervals. The geometry of the sonic anemometer setup disturbs the measurements for wind directions from 330° to 50° (see also App. D). Data for these wind directions are removed from the analysis.

3.2 VAD turbulence measurements

Methods to retrieve turbulence parameters from VAD scans are well-known and a variety of different methods exist. The method we refine in this study is based on the theory that was originally described by Eberhard et al. (1989) for lidar measurements. The variance of radial velocities σ_r^2 depends on the range gate distance R, the azimuth angle θ and the elevation angle φ. It is calculated from the measured radial ~~wind speeds~~ velocities V_r:

$$v_r(R,\theta,\varphi,t) = V_r(R,\theta,\varphi,t) - \langle V_r(R,\theta,\varphi)\rangle \tag{1}$$

$$\sigma_r^2 = \langle v_r(R,\theta,\varphi,t)^2\rangle \tag{2}$$

From a partial Fourier decomposition (see App. A) and for the special case of $\varphi = 35.3°$ a simple equation for E_{TKE} is derived:

$$E_{\mathrm{TKE}} = \frac{3}{2}\overline{\sigma}_r^2|_{\varphi=35.3°} \quad . \tag{3}$$

In this equation, $\overline{\sigma}_r^2$ is the mean of the variance of radial velocites over all azimuth angles. In the following, we will refer to this method as E89-retrieval.

In order to retrieve estimations of TKE dissipation rate ε from VAD scans, a similar approach to the method for sonic anemometers can be followed. A fit of the equation

$$D_r(\psi) = (4/3)C_K(\varepsilon\psi R')^{2/3} \quad , \tag{4}$$

to the azimuth structure function ~~to the equation~~

~~$D_r(\psi) = (4/3)C_K(\varepsilon\psi R')^{2/3}$,~~

with D_r the transverse structure function of radial velocities, C_K the Kolmogorov constant, ψ the azimuth angle increment and $R' = R\cos\varphi$ retrieves an estimate for ε according to Smalikho and Banakh (2017). We will refer to this method as S17A in the following.

Scanning with Doppler lidar in a ~~VAD implies~~ classical VAD with continuous motion of the azimuth motor involves a volume averaging of radial velocities in longitudinal ~~and transversal~~ (along the laser beam) and transverse (orthogonal to the beam) direction. The E89 and S17A methods do not consider this effect and will thus yield a systematic underestimation of TKE and ε. Smalikho and Banakh (2013) proposed a theory that considers the volume averaging and allows the retrieval of ε from conical scans, independent of the elevation angle. In Smalikho and Banakh (2017), this method has been combined with the E89-method to yield TKE, ε and the momentum fluxes. It is based on the decomposition of radial ~~wind speed~~ velocity variance σ_r^2 into its subcomponents, i.e.

$$\sigma_L^2 = \sigma_a^2 + \sigma_e^2 \quad , \tag{5}$$

$$\sigma_a^2 = \sigma_r^2 - \sigma_t^2 \quad , \tag{6}$$

$$\sigma_r^2 = \sigma_L^2 + \sigma_t^2 - \sigma_e^2 \tag{7}$$

where σ_L^2 ~~as~~ is the lidar measured variance, σ_a^2 as the lidar measured variance without instrumental error σ_e^2, and the turbulent broadening of the lidar measurement σ_t^2. In Smalikho and Banakh (2017), all of these variances and structure functions are calculated for single azimuth angles and then averaged. We describe in Sect.3.2.1 why we use total variances and structure functions of all radial velocities.

$\sigma_L^2 \quad = \sigma_a^2 + \sigma_e^2$

$\sigma_a^2 \quad = \sigma_r^2 - \sigma_t^2$

$\sigma_r^2 \quad = \sigma_L^2 + \sigma_t^2 - \sigma_e^2$

~~Additionally, the~~ The measured azimuth structure function $D_a(\psi_l)$ ~~(as~~ is a function of the separation angle ψ_l, where l is the index of the discrete separation angle of the scan~~)~~. It can be decomposed into the lidar measured structure function $D_L(\psi_l)$ and the instrumental error σ_e^2:

$D_a(\psi_l) = D_L(\psi_l) - 2\sigma_e^2$

$$D_L(\psi_l) = \langle [v_r(\theta) - v_r(\theta + \psi_l)]^2 \rangle \tag{8}$$

$$D_a(\psi_l) = D_L(\psi_l) - 2\sigma_e^2 \tag{9}$$

~~Substituting σ_e^2 in~~ Combining Eq. 8 with Eq. 9 yields:

$$\sigma_r^2 = \sigma_L^2 + \sigma_t^2 - \frac{1}{2} D_L(\psi_l) + \frac{1}{2} D_a(\psi_l) \quad . \tag{10}$$

~~With $\langle v_r^2 \rangle = \sigma_r^2$ in~~ It shows that since the instrumental error σ_e^2 is assumed to be a constant offset of azimuth structure function $D_a(\psi_l)$ and the lidar measurement $D_L(\psi_l)$, l can be chosen arbitrarily here. It is set to $l = 1$ because potential random errors like unstationary flow will be least effective for small separation angles. Using Eq.3 and Eq. 21 (see Sect.3.2.1), TKE can be redefined as a function of the measured line of sight variances σ_L^2, the measured lidar azimuth structure function of radial velocities $D_L(\psi_1)$ and a residual term G, which includes the two unknowns σ_t^2 and $D_a(\psi_1)$:

$$E_{\mathrm{TKE}} = \frac{3}{2} \left[\sigma_L^2 - \frac{D_L(\psi_1)}{2} + G \right] \quad , \tag{11}$$

$$G = \sigma_t^2 + \frac{1}{2} D_a(\psi_1) \tag{12}$$

In Banakh and Smalikho (2013), a relationship between the two unknowns and TKE dissipation rate is theoretically derived from the two-dimensional Kolmogorov-Obhukov spectrum as

$$\sigma_t = \varepsilon^{2/3} F(\Delta y) \tag{13}$$

$$D_a(\psi_l) = \varepsilon^{2/3} A(l \Delta y) \quad , \tag{14}$$

where $F(\Delta y)$ and $A(l\Delta y)$ are model functions that include the lidar filter functions (see App. B). The lidar filter functions in longitudinal direction depend on pulse width of the laser beam Δp and the time window T_w of the data acquisition. The transverse filter function is defined by $\Delta y = R\Delta\theta\cos\varphi$, which is the distance the lidar beam moves along the cone during one accumulation period. The parameters for the lidars in this study are provided in Tab. 1 and are calculated from information given by the manufacturer for the specific lidar type. Hence, G depends on the turbulence dissipation rate ε:

$$G = \varepsilon^{2/3}\left[F(\Delta y) + \frac{A(\Delta y)}{2}\right] \tag{15}$$

~~From~~ Using Eq. 14 and 9, ε can be retrieved ~~by the relation of measured differences in the structure function and the model structure function~~from $D_a(\psi_l) - D_a(\psi_1)$:

$$\varepsilon = \left[\frac{D_L(\psi_l) - D_L(\psi_1)}{A(l\Delta y) - A(\Delta y)}\right]^{3/2} \tag{16}$$

This equation does not depend on the elevation angle, so that the method allows the retrieval of ε from VAD scans with ~~other elevation angles~~ elevation angles different from 35.3° as well. Figure 3 gives an example of the different structure functions that are calculated in this method (i.e. D_L, D_a and A) and also gives a comparison to the structure function D_s as calculated from sonic anemometer measurements. ~~The value of $l = 9$ is chosen following the example of Smalikho and Banakh (2017) and corresponds to~~ Smalikho and Banakh (2017) found a separation angle of $l\Delta\theta = 9°$ ~~as it was found to be suitable in all conditions in that study~~an appropiate value for ABL measurements. In this study, all VAD scans are performed with a resolution of $\Delta\theta = 1°$, so that $l = 9$. In Fig. 3 the range that is thus used for the structure function fit is indicated by the bold black line. The retrieval method for ε using Eq. 16 and TKE using Eq. 11 will be referred to as S17 in the following.

3.2.1 Modifications for small number of scans

The VAD at $\varphi = 35.3°$ during the CoMet-campaign was not run continuously, but only six individual scans are performed successively before switching back to the VAD at $\varphi = 75°$ as described in Sect. 2.2. This means that only six data points are available to calculate variance and mean of the radial ~~wind speeds~~ velocities at each azimuth angle, which cannot be considered a solid statistic. We introduce two modifications of data processing to overcome this problem which are based on the assumptions of stationary and homogeneous turbulence.

Practical implementation of the ensemble average

In Eq. 2, $\langle V_r(R,\theta,\varphi)\rangle$ can be calculated as the arithmetic mean of radial ~~wind speeds~~ velocities at specific azimuth angles:

$$\langle V_r(R,\theta,\varphi)\rangle = \frac{1}{N}\sum_{n=0}^{N} V_r(R,\theta_n,\varphi) \quad , \tag{17}$$

where N is the number of scans. Instead of this approach, we suggest to use the reconstructed radial ~~wind speed~~ velocity from the retrieved wind field over all individual scans as the expected value in the variance calculation. For the retrieval of the

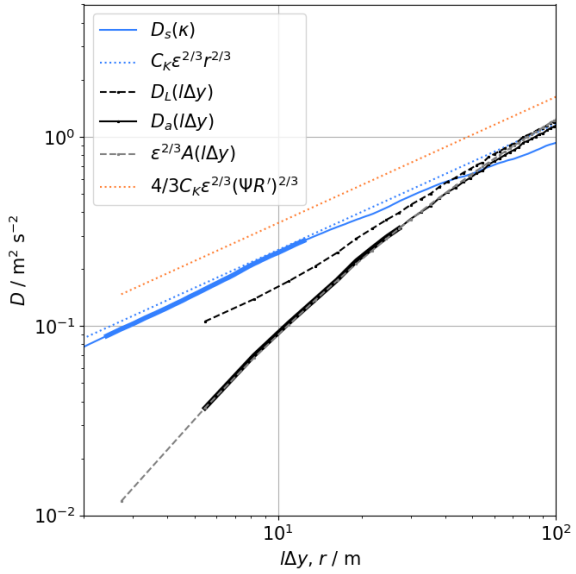

Figure 3. Example of structure functions of sonic anemometer (blue) and lidar (grey) at 90 m height on 4 April 2019, 1200-1230 UTC. The dashed black line shows the measured lidar structure function D_L, the solid black line D_a is corrected for the systematic error σ_e (see Eq. 9). The grey dashed line gives the model structure function A and the dotted lines indicate the reconstructed inertial subrange for the calculated values of ε. The parts with bold lines are those ranges that are used for the structure function fits.

three wind components ($\hat{u}$, $\hat{v}$, $\hat{w}$), filtered sine-wave fitting (FSWF) is applied (Smalikho, 2003). The reconstructed radial ~~wind speeds~~ velocities $\hat{V}$ are then used as the expected value in the variance calculation:

$$\hat{V} = \hat{w}(R)\sin\varphi + \hat{v}(R)\cos\varphi\cos\theta + \hat{u}(R)\cos\varphi\sin\theta \tag{18}$$

$$\langle V_r(R,\theta,\varphi)\rangle = \hat{V}(R,\theta,\varphi) \quad . \tag{19}$$

With this approach, all measurement points in the VAD with the same elevation angle are used to obtain the expected value $\langle V_r \rangle$ and thus, a better statistical significance is achieved. This method has also been proposed in Smalikho and Banakh (2017) as a practical implementation of Eq. 2.

Averaging of variances

In ~~(Smalikho and Banakh, 2017)~~Smalikho and Banakh (2017), the variances of the lidar measurements are defined as the average of variances at individual azimuth angles:

$$\overline{\sigma}_r^2 = \frac{1}{M}\sum_{\mathrm{m}=0}^{M}\sigma_r^2(\theta_m) \tag{20}$$

The variances $\sigma_r^2(\theta_m)$ are variances of a subsample of radial ~~wind speeds~~ velocities of the VAD (i.e. those at a specific azimuth angle θ_m). We use a simple relation between the variances of subsamples and the total variance of a dataset (see Appendix C). Applying this to the radial ~~wind speed~~ velocity variances yields:

$$\sigma_r^2 = \frac{k-1}{n-1} \sum\nolimits_{\text{j=1}}^{\text{m=1}} {}^{g}\sigma_r^2(\theta_m) + \frac{k(g-1)}{k-1}\overline{v}_r \quad , \tag{21}$$

where k is the number of samples at each azimuthal angle, g is the number of subsamples ~~(here: $g = 360$ for all azimuth angles)~~ and n is the number of total samples in the dataset ($n = gk$). Since the mean of the radial ~~wind speed fluctuations $\overline{v}_r = 0$~~ velocity fluctuations is zero by definition, ~~it is~~Eq. 21 becomes:

$$\sigma_r^2 \approx \overline{\sigma}_r^2(\theta_m) \quad . \tag{22}$$

3.2.2 Filtering of bad estimates

Improvements of turbulence estimates in low signal conditions can be achieved with filtering of bad estimates as described in Stephan et al. (2018). This approach is not based on the calculation of the azimuth structure function from measured radial ~~wind speeds~~velocities, but uses probability density functions (PDFs) and their corresponding standard deviations. The model PDF is defined as a Gaussian function with a filter term P:

$$p_M(x) = \frac{1-P}{\sqrt{2\pi}\sigma} \exp\left[-\frac{1}{2}\left(\frac{x}{\sigma}\right)^2\right] + \frac{P}{B_v} \quad , \tag{23}$$

where P is the probability of bad estimates of x, σ is the standard deviation of the PDF and B_v is the velocity bandwidth of the lidar. ~~Measured PDFs of the~~ For the measured variables $v_r(R,\theta)$, $\Delta v_r(R,\theta+\Delta\theta)$ and $\Delta v_r(R,\theta+l\Delta\theta)$~~are fit to the model PDFs to obtain an estimation of~~ , the best-fit model PDFs are found to to obtain the corresponding standard deviations σ_1, σ_2 and σ_3 and probability of bad estimates P_1, P_2 and P_3. However, since the PDFs cannot be assumed Gaussian in atmospheric turbulence, the standard deviations are finally calculated as the integral over the measured PDFs in the range $\pm 3.5\sigma$ according to Stephan et al. (2018).

Replacing σ_L^2 with σ_1^2, $D_L(\psi_1)$ with σ_2^2 and $D_L(\psi_l)$ with σ_3^2 in Eqs. 11 and 16 yields:

$$E_{\text{TKE}} = \frac{3}{2}\left[\sigma_1^2 - \frac{\sigma_2^2}{2} + G\right] \quad \text{and} \tag{24}$$

$$\epsilon = \left[\frac{\sigma_3^2 - \sigma_2^2}{A(l\Delta y) - A(\Delta y)}\right]^{3/2} \tag{25}$$

As suggested in Stephan et al. (2018), Eqs. 24 and 25 are only used if $P > 0$. We also introduced a quality control to discard any measurements with $P > 0.5$ for best results. In practice, this method will thus only be applied in some conditions when the signal is weak and can extend the range of vertical profiles to some degree.

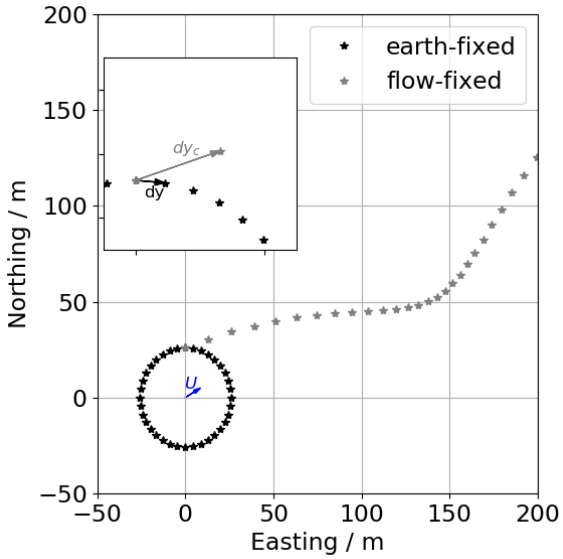

Figure 4. Sketch of measurement points of a VAD scan in an earth-fixed versus a flow-fixed coordinate system.

3.2.3 Correction for advection

The azimuth structure function and the volume average filter are distorted by advection through a modification of Δy. The effect is illustrated in Fig. 4. It shows that the distance between measurement points in a flow-fixed coordinate system is unequally spaced and on average larger than in the earth-fixed coordinate system. We propose a simplified correction~~as follows:~~. When advection is not considered, the spacing between samples is given by

$$\begin{aligned}
\Delta y &= \Delta\theta R\cos\varphi \\
\Delta y &\approx \tfrac{1}{N}\textstyle\sum_{i=0}^{N}\sqrt{dx_i^2+dy_i^2} \\
dx_i &= x_{\mathrm{i+1}} - x_i \\
dx_{\mathrm{c,i}} &= dx_i + \cos\Psi U\Delta t \\
dy_{\mathrm{c,i}} &= dy_i + \sin\Psi U\Delta t \\
\Delta y_c &\approx \tfrac{1}{N}\textstyle\sum_{i=0}^{N}\sqrt{dx_{\mathrm{c,i}}^2+dy_{\mathrm{c,i}}^2}\quad .
\end{aligned}$$

$$\Delta y = \Delta\theta R\cos\varphi \quad . \tag{26}$$

An estimate of the mean spacing can be obtained from

$$\Delta y \approx \frac{1}{N}\sum_{i=0}^{N}\sqrt{dx_i^2 + dy_i^2} \quad , \tag{27}$$

where $dx_i = x_{i+1} - x_i$. We propose a simplified correction in which

$$\Delta y_c \approx \frac{1}{N}\sum_{i=0}^{N}\sqrt{dx_{c,i}^2 + dy_{c,i}^2} \quad , \tag{28}$$

where

$$dx_{c,i} = dx_i + \cos\Psi U \Delta t \tag{29}$$

$$dy_{c,i} = dy_i + \sin\Psi U \Delta t \tag{30}$$

(31)

Here, R is the range gate distance, φ is the elevation angle, x_i and y_i are the measurement point locations , Ψ is wind direction, U is wind speed and Δt is the accumulation time of the lidar. The terms $\cos\Psi U\Delta t$ and $\sin\Psi U\Delta t$ describe the effect of advection on the measurement location in x- and y-direction respectively. Using the corrected measurement location displacements $dx_{c,i}$ and $dx_{c,i}$, we can calculate a corrected mean transverse sensing volume Δy_c. This method does not account for the unequal spacing, but corrects the average separation of data points, which is particularly important for the statistical evaluation of turbulence.

The effects of advection on the turbulence estimation is largest in the lowest levels of the VAD-scans, because Δy is small compared to $U\Delta t$ in this case. The retrieval method including the filtering for bad estimates, and the advection correction is referred to as ~~W19~~ W20 in the following.

3.2.4 Quality control filters

In order to fulfill the assumptions that are made with regards to the turbulence model and the turbulence retrieval method, the data is filtered according to the criteria given in Smalikho and Banakh (2017):

$$l\Delta y \ll L_v \quad , \tag{32}$$

$$L_v > \max\{\Delta z, \Delta y\} \tag{33}$$

$$R'\omega_s \gg |\langle \mathbf{V} \rangle| \tag{34}$$

For the purpose of evaluating the methods in a broad range, we set mild criteria for Eq. 32 and 34 using

$$l\Delta y < 2L_v \quad \text{and} \tag{35}$$

$$R'\omega_s > 2|\langle \mathbf{V} \rangle| \quad . \tag{36}$$

Table 2. Overview of turbulence retrieval methods and the applied filters and methods

	E89	S17A	S17	~~W19~~ W20
TKE	yes	yes	yes	yes
ε	no	yes	yes	yes
lidar volume averaging effect	no	no	yes	yes
CNR filter	yes	yes	yes	no
filter of bad estimates	no	no	no	yes
integral length scale filter	yes	yes	yes	yes
advection filter	no	no	yes	no
advection correction	no	no	no	yes
variance modifications	yes	yes	yes	yes

Equations 32 and 33 are criteria that require the integral length scale L_v to be larger than the sensing volume of the lidar in transversal (Δy) and longitudinal (Δz) direction. Unfortunately, there is no independent measurement of L_v at all heights of the VAD scan, so that it is derived from the lidar measurement itself as $L_v = 0.3796 \frac{E^{3/2}}{\varepsilon}$(Smalikho and Banakh, 2017).

The filter criteria in Eq. 34 is a filter for conditions with significant advection which distorts the measured structure functions and is only applied if the method described in Sect.3.2.3 is not used.

Except for the retrieval method ~~WS19~~W20, which uses the filtering of bad estimates, we set fixed CNR filter thresholds adapted to the lidar type. Since the turbulence retrievals are very sensitive to bad estimates, we set the CNR thresholds to conservative values that are given in Tab. 1.

An overview of all retrieval methods and their characteristics and filters that are applied is given in Tab. 2.

3.3 Turbulence estimation from airborne data

The estimation of turbulence parameters from the wind measurement system on the DLR Cessna Grand Caravan 208B (Mallaun et al., 2015) is done very similarly to the in-situ estimations from the sonic anemometer. TKE is calculated from the sum of variances as described in Sect. 3.3. Dissipation rate is also calculated from the second order structure function, but with different bounds for the time lag. For the flight data we use $\tau_1 = 0.2$ s and $\tau_2 = 2$ s, corresponding to approximately 13-130 m lag at 65 $\mathrm{m\,s^{-1}}$ mean airspeed.

To evaluate the heterogeneity of turbulence due to changing land use along the flight legs of more than 50 km length, we divided the legs into sub-legs of 6.5 km (i.e. 100 s averaging time) and calculate turbulence for each leg individually. The location of the legs and the sublegs is shown in Fig. 2.

4 Validation

4.1 Comparison to sonic anemometer

Best possible validation of the methods introduced in Sect. 3 can be performed with the lidar in close proximity to the meteorological mast such as at the measurement site at MOL-RAO. The sonic anemometers at 50 m and 90 m on the mast almost coincide with measurement levels of the lidar at 52 m and 93.6 m respectively. Since the VAD-retrieval with elevation angle of 35.3° yields TKE as well as its dissipation rate, both turbulence parameters can be compared to values obtained from the sonic anemometers. In this section we will evaluate the methods described in Sect. 3.2 and in particular the validity of the assumptions made in Sect. 3.2.1 and the efficiency of the advection correction described in Sect. 3.2.3.

4.1.1 Validation of modified variance

In Sect. 3.2.1 we introduced two modifications on the calculation of the averaged lidar radial ~~wind speed~~ velocity variances. These changes are especially necessary if a low number of VAD scans is used for turbulence retrieval. In the MOL-RAO experiment, VAD scans are run continuously with $\varphi = 35.3°$, so that the modifications can be tested against the original version of the retrieval method. The sonic anemometer at 90 m of the meteorological mast serves as an independent validation measurement. Figure 5a shows a time series of the two methods and the sonic anemometer in a time period in which all systems were providing good data almost without interruption (22 April - 29 April 2019). The lidar retrieval with both variance methods follows the sonic anemometer TKE estimation very well through the diurnal cycles, with some occasional overestimation that will be discussed in Sect. 4.1.2. Figure 5b gives the difference (ΔTKE) between azimuth average and total average to show that it is typically below 0.5 $\mathrm{m^2 s^{-2}}$ except for some periods with strong gradients in TKE. Figure 5c shows the scatterplot which directly compares the S17 retrieval calculated with azimuth averaged variances to the S17 retrieval using total variances. There is a higher estimation of TKE in the total variance method which increases with TKE. We cannot fully explain this effect at this point, but it might be due to the small scale turbulence that cannot be resolved with the 72 s sampling rate of radial ~~wind speeds~~ velocities at individual azimuth angles. It is small enough to be neglected for further analysis.

4.1.2 Comparison of lidar retrievals

The MOL-RAO dataset allows us to compare the retrievals without consideration of lidar volume averaging (E89 and S17A) to the S17 retrieval and its modified version ~~W19~~ W20 introduced in this study. For this purpose, the individual retrieval results are compared to the sonic anemometer estimates of TKE and its dissipation rate ε. Figure 6 shows the scatter plots for TKE at the two measurement levels. For each method, the coefficient of determination R_c^2 of the linear regression between sonic measurement and lidar retrieval is given, as well as a bias which is calculated as $b = \overline{(y - x)}$ for TKE and $b_{\log} = \overline{(\log_{10} y - \log_{10} x)}$ for ε. We find that with the E89-method, TKE is systematically underestimated, as expected. In contrast to that, the S17-method yields slightly overestimated TKE-values, if no advection filter is applied (light red dots), but a good agreement with the sonic anemometer in the absence of advection (red dots). The overestimation of TKE is larger for the lower level at 50 m compared

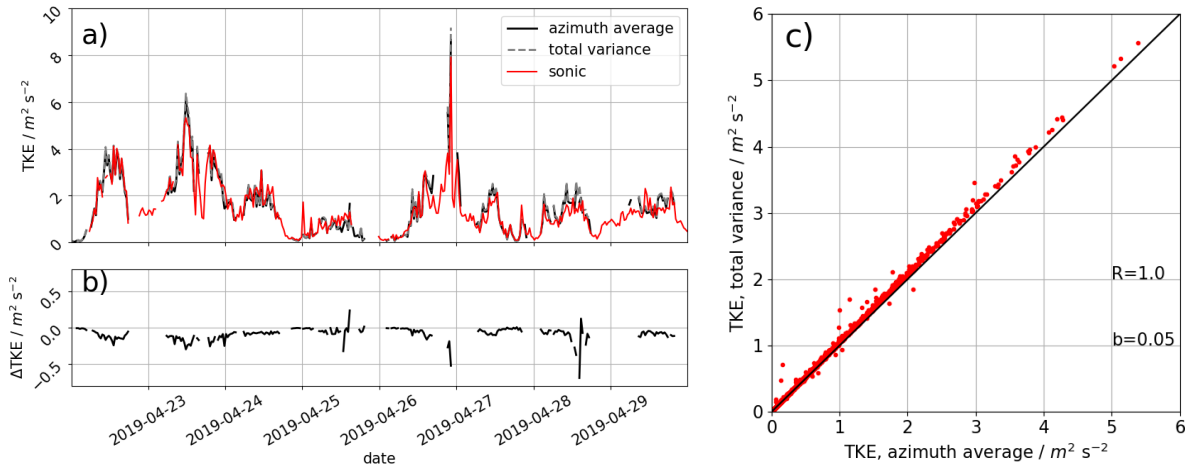

Figure 5. Time series of TKE from lidar retrievals compared to a sonic anemometer at 90 m above ground level (a)~~and scatterplot comparing~~ , the differencec between the lidar retrieval with averaged variances (Eq. 20) at specific azimuth angles θ to the modified, total variance method (Eq. 21) (b) and the scatterplot for the whole experimental period (c).

to the 90-m level which we attribute to the smaller averaging volume Δy. Our refined version of the retrieval, including the advection correction improves the results slightly and especially for the high turbulence cases (corresponding to high wind speeds) at the 50-m level, as the scatterplots show. Figure 7 gives the scatterplot comparison of ε-retrieval from S17A, S17 and ~~W19~~ W20 with the sonic anemometer respectively. E89 does not provide an estimate for ε. Even more clearly than for TKE, the underestimation of the method without consideration of lidar volume averaging (S17A) is found. Also, a now positive bias of $b = 0.09\ m^2\ s^{-2}$ of lidar estimates with the S17-method at the 50-m level is reduced with the advection correction to $b = 0.06\ m^2\ s^{-2}$. It is evident from the ε-estimates that all lidar retrievals underestimate turbulence significantly compared to the sonic anemometer in the low turbulence regimes, and in particular for values smaller than ~~10^{-3} m^2 s^{-3}~~$2 \cdot 10^{-3}$ m^2 s^{-3}, which is why these values have been excluded for the estimation of biases (grey dots).

4.1.3 Evaluation of advection error

To evaluate the error that is caused by advection in the S17-retrieval, all data that was collected at MOL-RAO was binned into wind speeds with a bin-width of 1 m s^{-1}. The mean absolute error between the lidar retrievals and the sonic anemometers at the respective level is calculated and shown in Figure 8 for TKE and ε. Although the averaged errors of TKE are small in general, it shows that the ~~W19-method~~ W20-method does reduce the error in comparison to the S17 method at the 50-m level. The error for ε at the 50-m level increases with wind speed, but less for the ~~W19-method~~W20-method. Hardly any improvement is found for the already small errors of TKE and ε at 90 m.

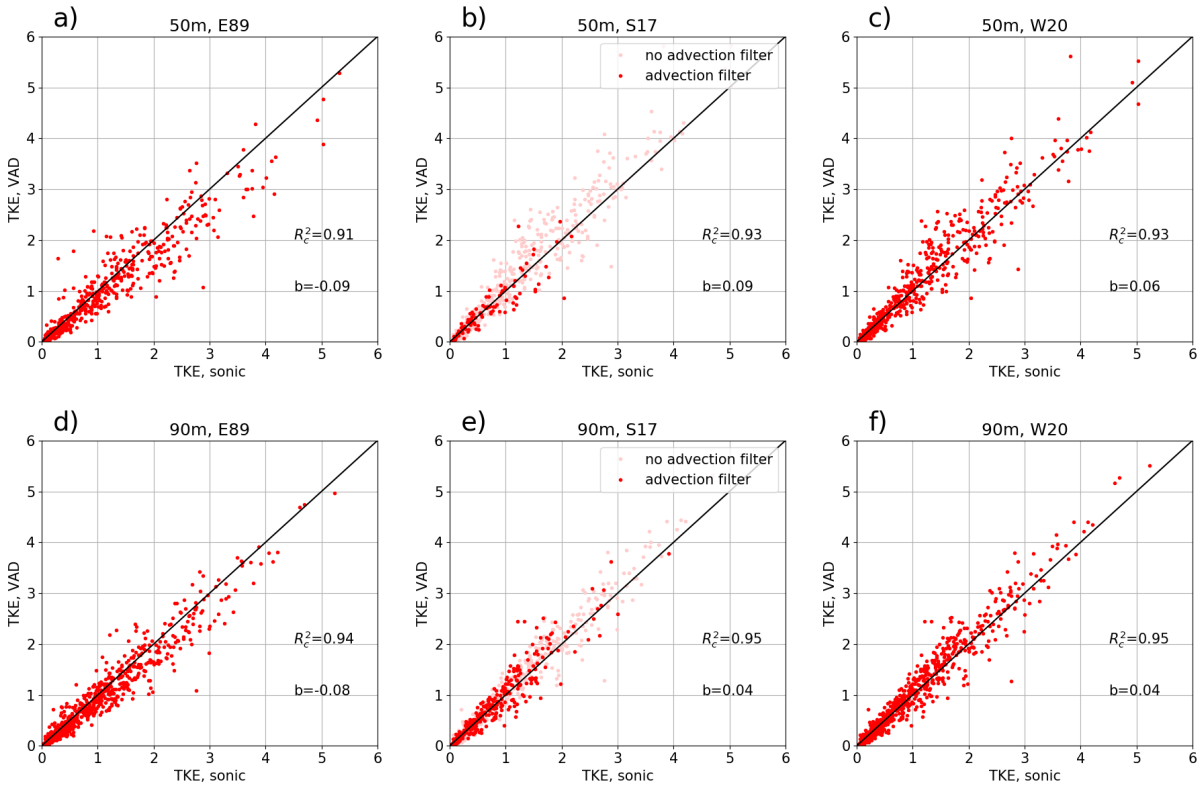

Figure 6. Scatter plot of lidar TKE retrieval against sonic anemometer TKE at 50-m level (a-c) and 90-m level (d-f). E89-retrieval is shown in (a) and (d), S17-retrieval in (b) and (e) and ~~W19-retrieval~~ W20-retrieval in (c) and (f). The light red dots in (b) and (e) show all TKE estimates without filter for advection, the dark red dots have the advection filter applied.

4.2 Comparison of elevation angles

VAD-scans with 35.3° allow to retrieve TKE as well as momentum fluxes using the methods described in Sect. 3. The disadvantage compared to VAD scans with larger elevation angles is that at the same range of the lidar line-of-sight measurement, lower altitudes are reached. If the limit of range is not given by the ABL height in any case, this can lead to significantly lower data availability at the ABL top. Another advantage of greater elevation angles is that the horizontal area that is covered with the VAD and thus the footprint of the measurement is much smaller than with low elevation angles. From the theory derived in Sect. 3.3, we see that the dissipation rate retrieval does not depend on the elevation angle and can thus be obtained from VAD scans with 75° elevation angle as well if the assumptions of isotropy and homogeneity hold. However, since the VAD at 75° has the more narrow cone, the separation distances Δy at respective measurement heights are smaller and thus the sensitivity to advection errors is expected to be larger. The measurements with two different elevation angles at the CoMet-campaign allow to compare dissipation rate retrievals for both kinds of VAD scans with the restriction that they are not simultaneous, but

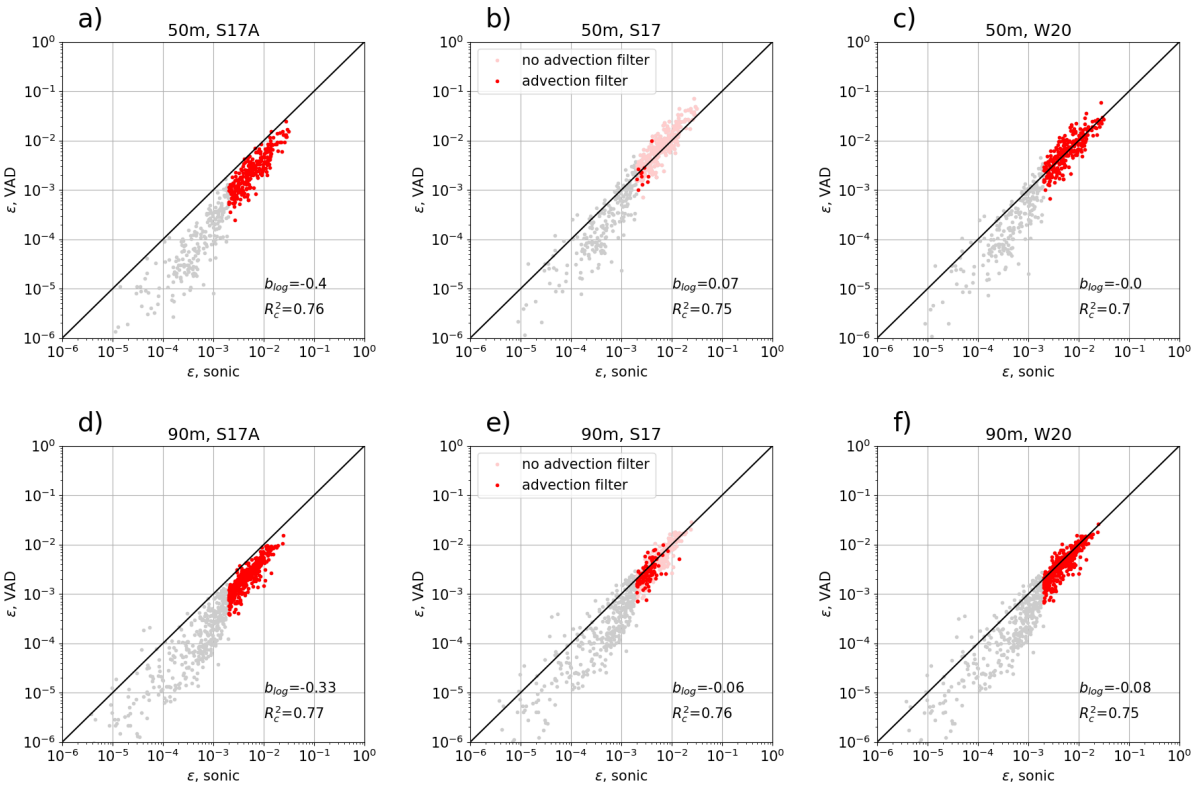

Figure 7. Scatter plot of lidar dissipation rate retrieval against sonic anemometer dissipation rate. The light red dots in (b) and (e) show the results without advection filter. The light grey dots are all estimates below $2 \cdot 10^{-3}$ $\mathrm{m^2 s^{-3}}$. Grey dots are not used for calculation of R nd $b_{\log}$.

sequential.

Figure 9 shows the comparison of both types of VADs in scatter plots of three measurement heights for the whole campaign period and ~~DLR~~DWL#1. In general, a large scatter is found between the two types of VAD which can be attributed to the different measurement times, different footprint and heterogeneous terrain. Applying a filter for significant advection as described in Sect. 3.2.4 removes most of the measurement points at the 100 m level in the 75° VAD. Without the filter (grey and red points), large, systematic overestimation against the VAD at 35.3° is found, which can still be seen at 500 m, but is not found at 1000 m any more. With the advection correction of ~~W19~~W20, the systematic error is reduced, but the random errors remain.

As for the comparison with the sonic anemometer, we evaluate the error in dependency of wind speed by binning the data in wind speeds between 0 $\mathrm{m\,s^{-1}}$ and 10 $\mathrm{m\,s^{-1}}$ (see Fig. 10). A clear trend is found for the 100 m-level which can be significantly reduced with the ~~W19~~ W20 method. A very small difference between the two elevation angles at the 500-m level is only reduced very little in the ~~W19~~ W20 method.

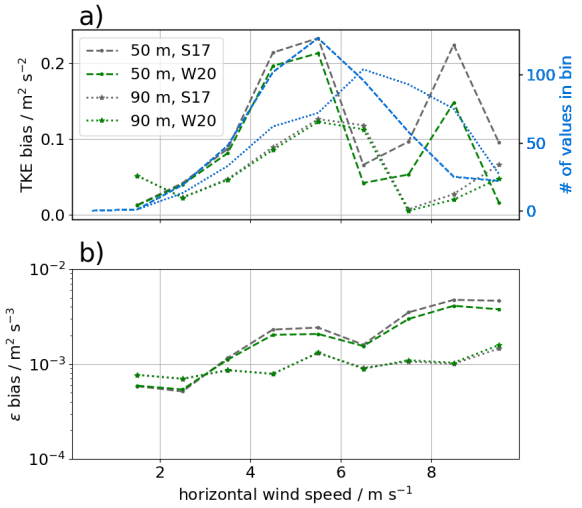

Figure 8. Difference of lidar retrieval of TKE (a) and TKE dissipation rate (b) compared to sonic anemometer as a function of wind speed.

4.3 Comparison to D-FDLR

At CoMet, no meteorological tower with sonic anemometers on levels that could be compared to the Doppler lidars was available. Instead, the aircraft D-FDLR was operating with a turbulence probe and provided in-situ turbulence data. On 5 June 2018, the aircraft was flying a so-called 'wall'-pattern, with long, straight and level legs at five altitudes (800 m, 1000 m, 1100 m, 1300 m and 1600 m). At least the lowest three levels of this flight allow a comparison to measurement levels of the top levels of lidar measurements on this day. Figure 11 shows the measured TKE of D-FDLR in the five flight levels. Only at the lowest two light levels (i.e. 800 m and 1000 m), significant turbulence is measured, with strong variations along the flight path.

Figure 12 shows the measurements from D-FDLR and the lidars ~~DLR~~DWL#1 and ~~DLR~~DWL#3 that were taken between 1400 and 1530 UTC as vertical profiles. The solid red line gives the average of all sub-legs along the 50 km flight of D-FDLR, and the shaded areas give the range between the minimum and the maximum at each height. It shows nicely how the measurements of turbulence at the ~~DLR~~DWL#3-site are significantly lower than at ~~DLR~~DWL#1, which we attribute to the lake fetch. The D-FDLR measurements of TKE almost match with the ~~DLR~~DWL#1 site and are all higher than at the ~~DLR~~DWL#3-site, which fits to the environmental conditions of heterogeneous land-use. Figure 12a also gives the comparison between E89-, S17- and ~~W19-estimates~~ W20-estimates of the same dataset. Here, it shows that the difference between S17 and ~~W19~~ W20 only occurs at the very lowest level, but the underestimation of the E89-method is found up to 750 m. In dissipation rate estimates, the ~~DLR~~DWL#1 measurements are at the low end of the range that was measured with D-FDLR and the lake-site measurements are even smaller. The estimates from 35.3°-scans and 75°-scans agree very well, especially at the higher levels, which shows that the assumption of isotropy and homogeneity seem to hold. The presumed underestimation of

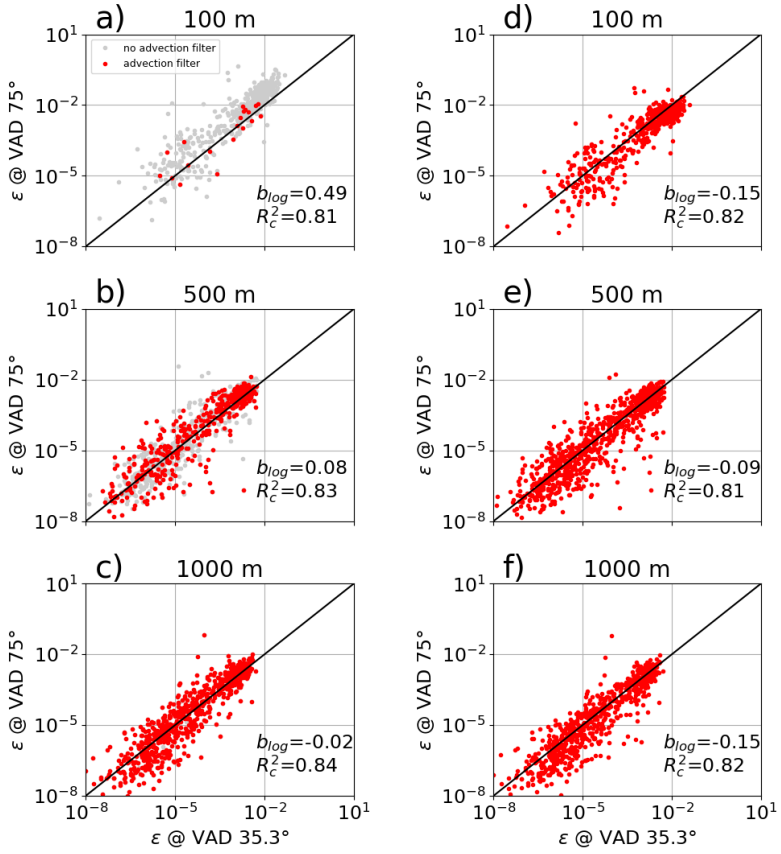

Figure 9. Scatter plot of lidar dissipation rate retrieval from VAD scans with 75° elevation angle versus 35.3°. On the left, retrievals without advection correction are shown for the three different levels (a) 100m, (b) 500m and (c) 1000m. On the right the corresponding scatter plots with advection correction are presented (d-f).

ε of lidar retrievals compared to in-situ measurements at absolute values of 10^{-3} $\mathrm{m^2\,s^{-3}}$ is consistent to what was found for the comparison to sonic anemometer measurements. This single case of airborne measurements compared to lidar retrievals at higher altitudes can however not provide any statistical validation.

Figure 13 shows measurements of ε retrieved with the ~~W19-method~~ W20-method for the VAD scans with 75° elevation and all three lidars. It shows that the growth of the boundary-layer with its increased turbulence can be nicely captured by the lidars. There are some differences between the three locations, especially lower turbulence close to the ground at the ~~DLR~~DWL#3-location and a higher boundary layer at the ~~DLR~~DWL#2 location. More studies will be necessary in future, analyzing the data of the whole campaign to improve the understanding of land-atmosphere interaction in this case.

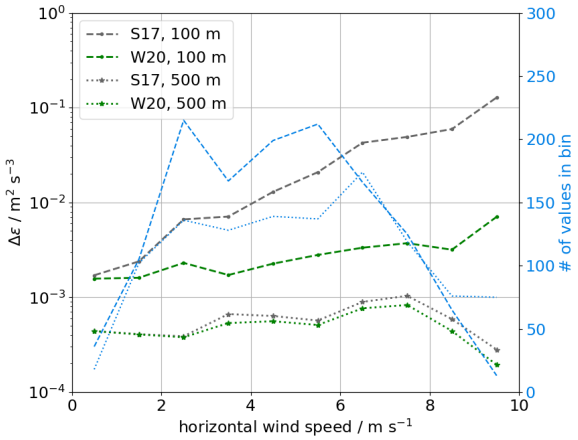

Figure 10. Difference of lidar ε-retrievals of both kinds of VAD as a function of wind speed.

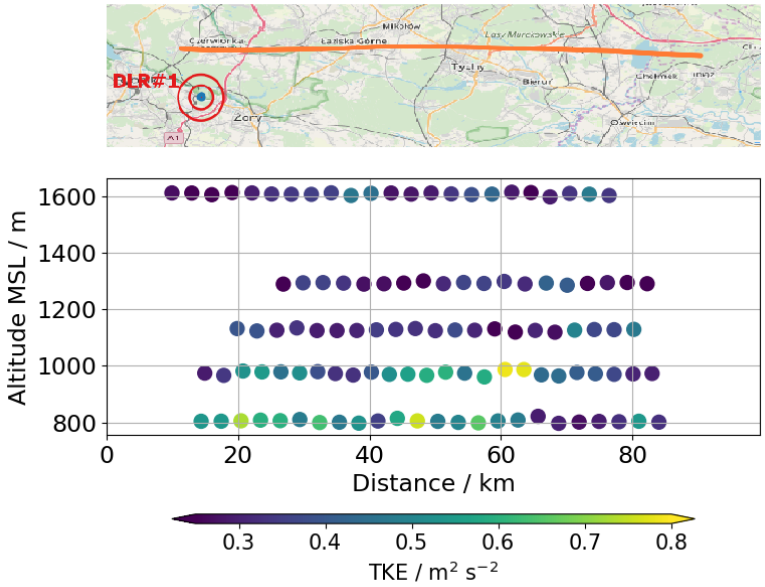

Figure 11. D-FDLR TKE measurements at five flight levels. Map data ©OpenStreetMap contributors 2019. Distributed under a Creative Commons BY-SA License.

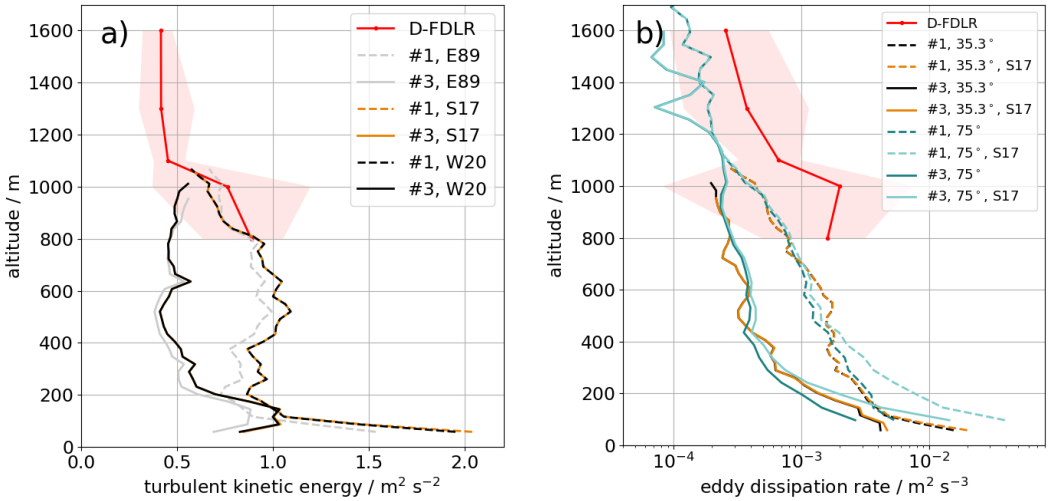

Figure 12. Vertical profile of TKE (left) and ε (right) compared to measurements by D-FDLR.

5 Conclusions

In this study, we used four different methods to retrieve turbulence from the same data obtained through lidar VAD scans. The MOL-RAO experiment allowed us to show that methods which do not account for the lidar volume averaging effect underestimate turbulence compared to sonic anemometers at 50 m and 90 m systematically. This has been shown for the first time with such a big dataset. The S17-method tackles this problem, but introduces an overestimation in our dataset. Parts of this overestimation can be attributed to advection, which distorts the retrieval of the azimuth structure function and the transverse filter function in the lidar model. The advection effects are ~~most~~ relevant at the lowest measurement heights where the spatial separation of lidar beams along the VAD cone Δy ~~are small.~~ is small. This effect is stronger than increasing wind speeds at higher altitudes in our observations. We propose a correction for this issue and show here that our method reduces the systematic errors compared to the sonic anemometers at the 50-m level. ~~It is also shown~~ To confirm that advection is the reason for this improvement we show that the bias increases with wind speed. With all retrievals, dissipation rates of values smaller than $10^{-3}\ \mathrm{m^2\,s^{-3}}$ are underestimated by the lidars, likely because the small scale fluctuations that are carrying much of the energy in these cases, cannot be resolved any more. A remaining piece of uncertainty are the lidar parameters Δp and T_w which are given by the manufacturer for the lidar type, but could potentially differ for individual lidars. Exact knowledge about these parameters could reduce the uncertainty of the model functions F and A (see App. B) and thus improve the corrections of the volume averaging effects. It is conceivable that the observed overestimation of the S17 (and ~~W19~~W20) based TKE can partly also be attributed to these uncertainties.

The aircraft measurements that were carried out during the CoMet campaign were used to show the agreement of the lidar retrievals with in-situ measurements at higher altitudes. It is the first time that these lidar measurements have been compared

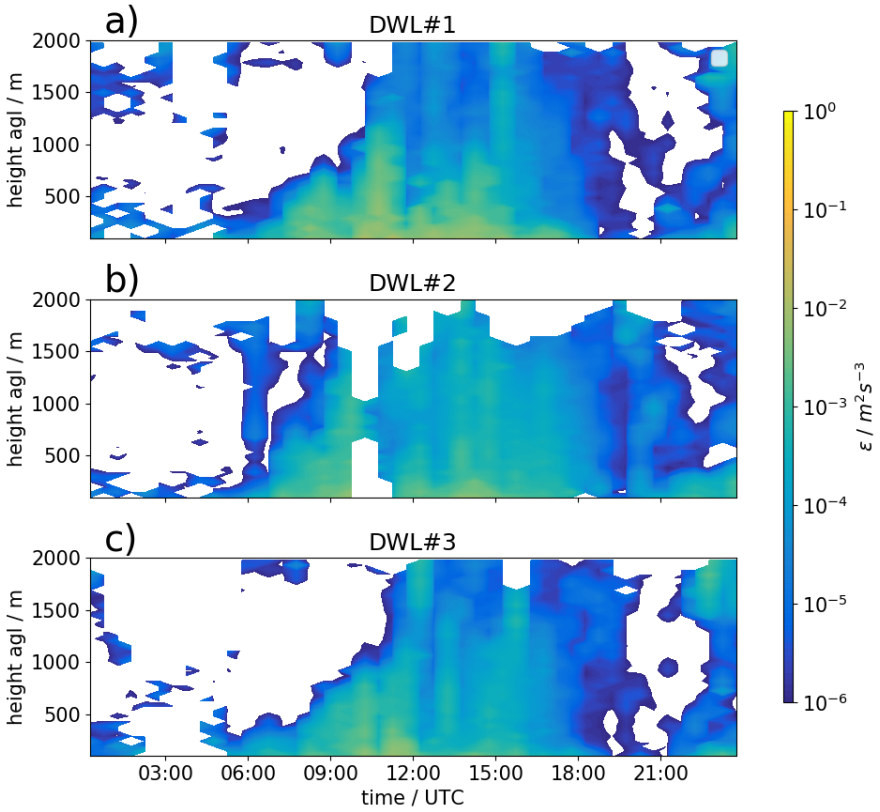

Figure 13. Diurnal cycle of TKE dissipation rate on 5 June 2018 at the three lidar locations calculated with the ~~W19-method~~W20-method.

to in-situ aircraft data. Unfortunately, only measurements of one day allowed a comparison and the spatial separation of the measurements introduces additional uncertainty. It was found that TKE estimates from lidar and aircraft compare rather well, but the small values of dissipation rates at these heights are underestimated by the lidar to a similar order of magnitude as for low turbulence conditions in the sonic anemometer comparison. Dedicated experiments will be necessary in future to provide more comprehensive validation datasets for turbulence retrievals with lidar VAD scans. Given the larger separation distances Δy of the lidar beams at higher altitudes, the assumption that $l\Delta y \ll L_v$ is more likely to be violated. Airborne in-situ measurements are the best way to validate the assumptions and the lidar retrievals in these cases.

The CoMet dataset was also used to show that with VAD-scans with larger elevation angle (here: 75°) can be used to retrieve TKE dissipation rate with the same method as for VAD-scans with 35.3° and the results are comparable. For this narrow VAD cone scans, we showed that the advection correction is much more important than for lower elevation angles and strong overestimation of ε can occur in conditions with high wind speeds if it is not applied. The distribution of three lidars in Upper Silesia in areas of different land-use shows the variability of turbulence and boundary-layer flow in this area. Using the VAD

scans with different elevation angle can in future potentially help to analyze horizontal heterogeneity in the boundary layer and its impact on the calculation of area-averaged fluxes.

Data availability. The data are available from the author upon request.

Appendix A: Fourier decomposition

Eberhard et al. (1989) show that radial ~~wind speed~~ velocity variance can be decomposed into the components u, v and w of the meteorological wind vector:

$$\begin{aligned}\langle v_r^2(R,\theta,\varphi)\rangle &= \langle [V_r(R,\theta,\varphi,t) - \langle V_r(R,\theta,\varphi)\rangle]^2\rangle \\ &= \frac{\cos^2\varphi}{2}\left[\langle u^2\rangle + \langle v^2\rangle + 2\tan^2\varphi\langle w^2\rangle\right] \\ &+ \sin 2\varphi\langle uw\rangle - \sin 2\varphi\langle vw\rangle\sin\theta \\ &+ \frac{\cos^2\varphi}{2}\left[\langle u^2\rangle + \langle v^2\rangle\right]\cos 2\theta - \cos^2\varphi\langle uv\rangle\sin 2\theta \end{aligned} \tag{A1}$$

A partial decomposition of Eq. A1 yields:

$$\begin{aligned}\langle u^2\rangle + \langle v^2\rangle + 2\tan^2\varphi\langle w^2\rangle &= \frac{1}{\pi\cos^2\varphi}\int_0^{2\pi}\langle v_r^2\rangle d\theta \\ &= \frac{2}{\cos^2\varphi}\langle\langle v_r^2\rangle\rangle_\theta \end{aligned} \tag{A2}$$

$$\langle uw\rangle = \frac{1}{\pi\sin^2\varphi}\int_0^{2\pi}\langle v_r^2\rangle\cos\theta d\theta \tag{A3}$$

$$\langle vw\rangle = \frac{-1}{\pi\sin^2\varphi}\int_0^{2\pi}\langle v_r^2\rangle\sin\theta d\theta \quad . \tag{A4}$$

These equations provide the basis for the retrieval of TKE and momentum fluxes from lidar VAD measurements.

Appendix B: Lidar filter functions

Theoretical models for the spectral broadening of lidar measurements ($F(\Delta y)$) and the structure function($A(l\Delta y)$) are derived in Banakh and Smalikho (2013) from the two-dimensional Kolmogorov spectrum for lidar measurements of turbulence:

$$\Theta(\kappa_z,\kappa_y) = C_3(\kappa_z^2+\kappa_y^2)^{-4/3}\left[1+\frac{8}{3}\cdot\frac{\kappa_y^2}{\kappa_z^2+\kappa_y^2}\right] \tag{B1}$$

$$F(\Delta y) = \int_0^\infty d\kappa_z \int_0^\infty d\kappa_y \Theta(\kappa_z,\kappa_y)\left[1-H_\parallel(\kappa_z)H_\perp(\kappa_y)\right] \tag{B2}$$

$$A(l\Delta y) = 2\int_0^\infty d\kappa_z \int_0^\infty d\kappa_y \Theta(\kappa_z,\kappa_y)H_\parallel(\kappa_z)H_\perp(\kappa_y)\left[1-\cos(2\pi l\Delta y_i\kappa_y)\right] \quad , \tag{B3}$$

where $H_\parallel$ is the longitudinal and $H_\perp$ the transverse filter function of lidar measurements in the VAD scan:

$$H_\parallel(\kappa_1) = \left[\exp\left[-(\pi\Delta p\kappa_1)^2\right]\frac{\sin(\pi\Delta R\kappa_1)}{\pi\Delta R\kappa_1}\right]^2 \tag{B4}$$

$$H_\perp(\kappa_2) = \left[\frac{\sin(\pi\Delta y\kappa_2)}{\pi\Delta y\kappa_2}\right]^2 \quad , \tag{B5}$$

where Δp is derived from the FWHM pulse width τ_p, ΔR from the time window T_w and Δy from the VAD azimuth increment $\Delta\theta$:

$$\Delta p = 0.5c\left(\frac{\tau_p}{2\sqrt{\log 2}}\right) \tag{B6}$$

$$\Delta R = 0.5cT_w \tag{B7}$$

$$\Delta y = R\Delta\theta\cos\varphi \tag{B8}$$

$$\tag{B9}$$

Appendix C: Sum of variance of subsamples

For statistically independent subsamples X_j with size k_j, the total variance of the dataset can be derived as follows:

$$E_j = \mathrm{E}[X_j] = \frac{1}{k_j}\sum_{i=1}^{k_j} X_{ji} \tag{C1}$$

$$V_j = \mathrm{Var}[X_j] = \frac{1}{k_j-1}\sum_{i=1}^{k_j}(X_{ji}-E_j)^2 \quad , \tag{C2}$$

where j is the index of the subsample and i the index of the element in the subsample.

$$\mathrm{Var}[X] = \frac{1}{n-1}\sum_{j=1}^{g}\sum_{i=1}^{k_j}(X_{ji} - \mathrm{E}[X])^2 \tag{C3}$$

$$= \frac{1}{n-1}\sum_{j=1}^{g}\sum_{i=1}^{k_j}\left((X_{ji} - E_j) - (\mathrm{E}[X] - E_j)\right)^2 \tag{C4}$$

$$= \frac{1}{n-1}\sum_{j=1}^{g}\sum_{i=1}^{k_j}(X_{ji} - E_j)^2 - 2(X_{ji} - E_j)(\mathrm{E}[X] - E_j) + (\mathrm{E}[X] - E_j)^2 \tag{C5}$$

$$= \frac{1}{n-1}\sum_{j=1}^{g}(k_j - 1)V_j + k_j(\mathrm{E}[X] - E_j)^2 \quad , \tag{C6}$$

where $n = \sum k_j$. Eventually, for equally sized subsamples one obtains:

$$\mathrm{Var}[X] = \frac{1}{n-1}\sum_{j=1}^{g}(k-1)V_j + k(g-1)\mathrm{Var}[E_j] \tag{C7}$$

$$= \frac{k-1}{n-1}\sum_{j=1}^{g}V_j + \frac{k(g-1)}{k-1}\mathrm{Var}[E_j] \tag{C8}$$

Appendix D: Validation of wind retrieval

The FSWF-retrieval is used to obtain the three-dimensional wind vector from the lidar VAD scans. The results of the retrieval is compared to the sonic anemometers at 50 m and 90 m and shown in Fig. D1. To show the distortion of the mast, no data have been removed in the retrieval of wind speed and wind direction for this figure.

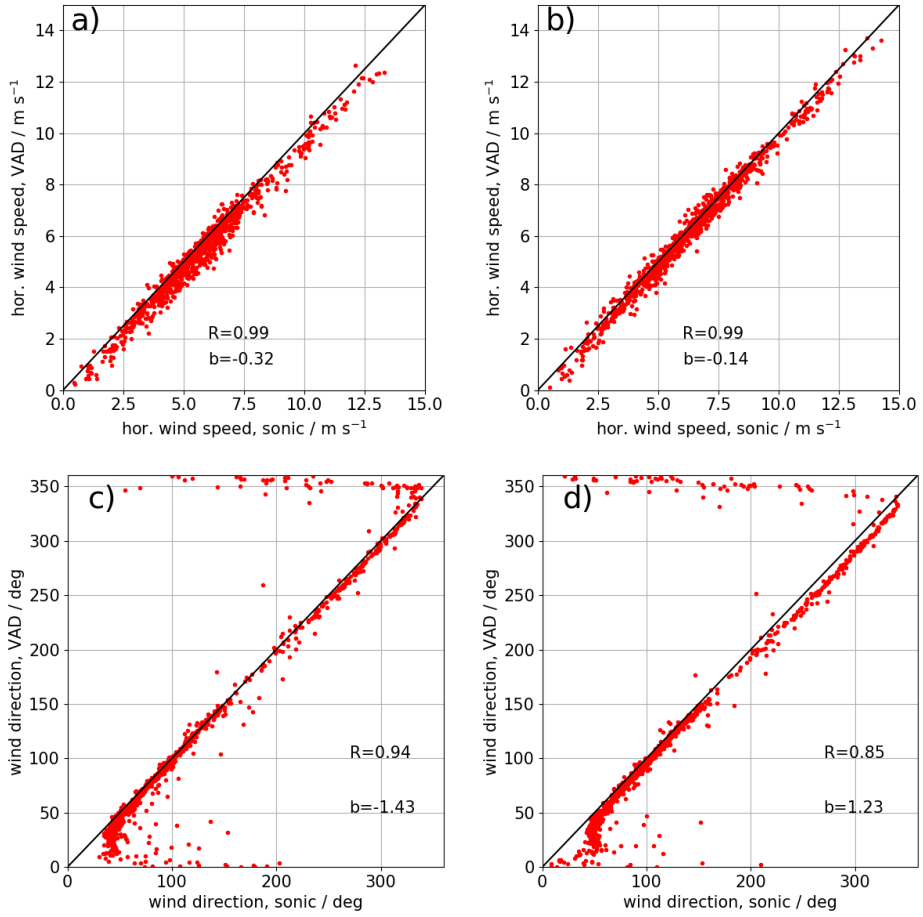

Figure D1. Scatter plot of horizontal wind speed retrieved from lidar measurements compared to sonic anemometer measurements at 50 m (a) and 90 m (b) and wind direction (c and d).

Appendix E: Nomenclature

λ	laser wavelength
τ_p	lidar pulse length (full width half maximum, FWHM)
T_w	lidar time window
φ	elevation angle
θ	azimuth angle
u	wind component towards East
v	wind component towards North
w	upward wind component
σ_u^2	u-wind component variance
σ_v^2	v-wind component variance
σ_w^2	w-wind component variance
τ_i	time separation
V_r	radial wind component
v_r	radial wind component difference from mean
σ_r^2	radial wind component variance
R	range gate distance
E_{TKE}	turbulence kinetic energy
ε	TKE dissipation rate
C_K	Kolmogorov constant
ψ	azimuth angle increment
κ	wave number
r	separation distance
σ_L^2	variance of lidar measurements
σ_e^2	lidar instrumental noise
σ_a^2	variance of lidar measurements without instrumental noise
σ_t^2	turbulent broadening of the Doppler spectrum
ΔR	distance between neighboring range gate centers
D_r	azimuth structure function
D_s	longitudinal structure function measured by sonic anemometer
D_L	lidar measurement of azimuth structure function
D_a	$D_L - 2\sigma_e^2$
A	theoretical model for azimuth structure function
F	theoretical model for turbulent broadening of the Doppler spectrum
Δy	distance of lidar beam movement during one accumulation period
Δy_c	modified Δy for advection
p_M	model PDF
P	probability of bad estimates
L_v	integral length scale
ω_s	angular velocity of VAD scan
Ψ	wind direction
U	horizontal wind speed
Δt	accumulation time
R_c	linear regression correlation coefficient
b	measurement bias

Author contributions. NW, EP, AR and CM helped design and carry out the field measurements. CM provided processed data from the D-FDLR aircraft turbulence probe. NW analyzed the data from the sonic anemometers, the profiling lidars and the D-FDLR. NW wrote the paper, with significant contributions from EP. All the coauthors contributed to refining the paper text.

Competing interests. The authors declare that they have no competing interests.

5 *Acknowledgements.* We want to thank Jarosław Nęcki and all of the students of the University of Science and Technology, Cracow for their tireless work in support of the CoMet campaign. We thank the Aeroklub Rybnickiego Okręgu Węglowego, Hotel Restauracja Pustelnik and Agroturystyka "Na Polanie" for providing space and infrastructure for the lidar deployment in Upper Silesia. We thank Frank Beyrich and Andreas Fix for internal reviews and their input to the manuscript.

References

Banakh, V. and Smalikho, I.: Coherent Doppler Wind Lidars in a Turbulent Atmosphere, Radar, Artech House, 2013.

Banakh, V. A., Smalikho, I. N., Köpp, F., and Werner, C.: Measurements of Turbulent Energy Dissipation Rate with a CW Doppler Lidar in the Atmospheric Boundary Layer, Journal of Atmospheric and Oceanic Technology, 16, 1044–1061, https://doi.org/10.1175/1520-0426(1999)016<1044:MOTEDR>2.0.CO;2, 1999.

Bange, J., Beyrich, F., and Engelbart, D. A. M.: Airborne Measurements of Turbulent Fluxes during LITFASS-98: A Case Study about Method and Significance, Theor. Appl. Climatol., 73, 35–51, 2002.

Beyrich, F., Leps, J.-P., Mauder, M., Bange, J., Foken, T., Huneke, S., Lohse, H., Lüdi, A., Meijninger, W., Mironov, D., Weisensee, U., and Zittel, P.: Area-Averaged Surface Fluxes Over the Litfass Region Based on Eddy-Covariance Measurements, Boundary-Layer Meteorol., 121, 33–65, https://doi.org/10.1007/s10546-006-9052-x, 2006.

Bodini, N., Lundquist, J. K., and Newsom, R. K.: Estimation of turbulence dissipation rate and its variability from sonic anemometer and wind Doppler lidar during the XPIA field campaign, Atmospheric Measurement Techniques, 11, 4291–4308, https://doi.org/10.5194/amt-11-4291-2018, 2018.

Eberhard, W. L., Cupp, R. E., and Healy, K. R.: Doppler Lidar Measurement of Profiles of Turbulence and Momentum Flux, Journal of Atmospheric and Oceanic Technology, 6, 809–819, https://doi.org/10.1175/1520-0426(1989)006<0809:DLMOPO>2.0.CO;2, 1989.

Fiehn, A., Kostinek, J., Eckl, M., Klausner, T., Galkowski, M., Chen, J., Gerbig, C., Röckmann, T., Maazallahi, H., Schmidt, M., Korben, P., Necki, J., Wildmann, N., Mallaun, C., Bun, R., Fix, A., and Roiger, A.: Estimating CH4, CO2, and CO emissions from coal mining and industrial activities in the Upper Silesian Coal Basin using an aircraft-based mass balance approach, Atmos. Chem. Phys., p. in preparation, 2020.

Frehlich, R., Meillier, Y., Jensen, M. L., and Balsley, B.: Turbulence Measurements with the CIRES Tethered Lifting System during CASES-99: Calibration and Spectral Analysis of Temperature and Velocity, Journal of the Atmospheric Sciences, 60, 2487–2495, https://doi.org/10.1175/1520-0469(2003)060<2487:TMWTCT>2.0.CO;2, 2003.

Fuertes, F. C., Iungo, G. V., and Porté-Agel, F.: 3D Turbulence Measurements Using Three Synchronous Wind Lidars: Validation against Sonic Anemometry, Journal of Atmospheric and Oceanic Technology, 31, 1549–1556, https://doi.org/10.1175/JTECH-D-13-00206.1, 2014.

Holtslag, A. A. M., Gryning, S. E., Irwin, J. S., and Sivertsen, B.: Parameterization of the Atmospheric Boundary Layer for Air Pollution Dispersion Models, pp. 147–175, Springer US, Boston, MA, https://doi.org/10.1007/978-1-4757-9125-9_11, 1986.

Kelberlau, F. and Mann, J.: Better turbulence spectra from velocity–azimuth display scanning wind lidar, Atmospheric Measurement Techniques, 12, 1871–1888, https://doi.org/10.5194/amt-12-1871-2019, 2019a.

Kelberlau, F. and Mann, J.: Cross-contamination effect on turbulence spectra from Doppler beam swinging wind lidar, Wind Energy Science Discussions, 2019, 1–28, https://doi.org/10.5194/wes-2019-71, 2019b.

Krishnamurthy, R., Calhoun, R., Billings, B., and Doyle, J.: Wind turbulence estimates in a valley by coherent Doppler lidar, Meteorological Applications, 18, 361–371, https://doi.org/10.1002/met.263, 2011.

Kropfli, R. A.: Single Doppler Radar Measurements of Turbulence Profiles in the Convective Boundary Layer, Journal of Atmospheric and Oceanic Technology, 3, 305–314, https://doi.org/10.1175/1520-0426(1986)003<0305:SDRMOT>2.0.CO;2, 1986.

Kumer, V.-M., Reuder, J., Dorninger, M., Zauner, R., and Grubisic, V.: Turbulent kinetic energy estimates from profiling wind LiDAR measurements and their potential for wind energy applications, Renewable Energy, 99, 898 – 910, https://doi.org/http://dx.doi.org/10.1016/j.renene.2016.07.014, 2016.

Liu, H., Peters, G., and Foken, T.: New Equations For Sonic Temperature Variance And Buoyancy Heat Flux With An Omnidirectional Sonic Anemometer, Boundary-Layer Meteorology, 100, 459–468, https://doi.org/10.1023/A:1019207031397, 2001.

Luther, A., Kleinschek, R., Scheidweiler, L., Defratyka, S., Stanisavljevic, M., Forstmaier, A., Dandocsi, A., Wolff, S., Dubravica, D., Wildmann, N., Kostinek, J., Jöckel, P., Nickl, A.-L., Klausner, T., Hase, F., Frey, M., Chen, J., Dietrich, F., Necki, J., Swolkień, J., Fix, A., Roiger, A., and Butz, A.: Quantifying CH_4 emissions from hard coal mines using mobile sun-viewing Fourier transform spectrometry, Atmospheric Measurement Techniques, 12, 5217–5230, https://doi.org/10.5194/amt-12-5217-2019, 2019.

Mallaun, C., Giez, A., and Baumann, R.: Calibration of 3-D wind measurements on a single-engine research aircraft, Atmospheric Measurement Techniques, 8, 3177–3196, https://doi.org/10.5194/amt-8-3177-2015, 2015.

Muñoz-Esparza, D., Sharman, R. D., and Lundquist, J. K.: Turbulence Dissipation Rate in the Atmospheric Boundary Layer: Observations and WRF Mesoscale Modeling during the XPIA Field Campaign, Monthly Weather Review, 146, 351–371, https://doi.org/10.1175/MWR-D-17-0186.1, 2018.

O'Connor, E. J., Illingworth, A. J., Brooks, I. M., Westbrook, C. D., Hogan, R. J., Davies, F., and Brooks, B. J.: A Method for Estimating the Turbulent Kinetic Energy Dissipation Rate from a Vertically Pointing Doppler Lidar, and Independent Evaluation from Balloon-Borne In Situ Measurements, Journal of Atmospheric and Oceanic Technology, 27, 1652–1664, https://doi.org/10.1175/2010JTECHA1455.1, 2010.

Pauscher, L., Vasiljevic, N., Callies, D., Lea, G., Mann, J., Klaas, T., Hieronimus, J., Gottschall, J., Schwesig, A., Kühn, M., and Courtney, M.: An Inter-Comparison Study of Multi- and DBS Lidar Measurements in Complex Terrain, Remote Sensing, 8, 782, https://doi.org/10.3390/rs8090782, 2016.

Smalikho, I.: Techniques of Wind Vector Estimation from Data Measured with a Scanning Coherent Doppler Lidar, Journal of Atmospheric and Oceanic Technology, 20, 276–291, https://doi.org/10.1175/1520-0426(2003)020<0276:TOWVEF>2.0.CO;2, 2003.

Smalikho, I., Köpp, F., and Rahm, S.: Measurement of Atmospheric Turbulence by 2-μm Doppler Lidar, Journal of Atmospheric and Oceanic Technology, 22, 1733–1747, https://doi.org/10.1175/JTECH1815.1, 2005.

Smalikho, I. N. and Banakh, V. A.: Accuracy of estimation of the turbulent energy dissipation rate from wind measurements with a conically scanning pulsed coherent Doppler lidar. Part I. Algorithm of data processing, Atmospheric and Oceanic Optics, 26, 404–410, https://doi.org/10.1134/S102485601305014X, 2013.

Smalikho, I. N. and Banakh, V. A.: Measurements of wind turbulence parameters by a conically scanning coherent Doppler lidar in the atmospheric boundary layer, Atmospheric Measurement Techniques, 10, 4191–4208, https://doi.org/10.5194/amt-10-4191-2017, 2017.

Stephan, A., Wildmann, N., and Smalikho, I. N.: Spatiotemporal visualization of wind turbulence from measurements by a Windcube 200s lidar in the atmospheric boundary layer, Proc.SPIE, 10833, 10 833 – 10 833 – 10, https://doi.org/10.1117/12.2504468, 2018.

van den Kroonenberg, A., Martin, S., Beyrich, F., and Bange, J.: Spatially-averaged temperature structure parameter over a heterogeneous surface measured by an unmanned aerial vehicle, Boundary-Layer Meteorol., 142, 55–77, 2011.

van Kuik, G. A. M., Peinke, J., Nijssen, R., Lekou, D., Mann, J., Sørensen, J. N., Ferreira, C., van Wingerden, J. W., Schlipf, D., Gebraad, P., Polinder, H., Abrahamsen, A., van Bussel, G. J. W., Sørensen, J. D., Tavner, P., Bottasso, C. L., Muskulus, M., Matha, D., Lindeboom, H. J., Degraer, S., Kramer, O., Lehnhoff, S., Sonnenschein, M., Sørensen, P. E., Künneke, R. W., Morthorst, P. E., and Skytte, K.: Long-term research challenges in wind energy –

a research agenda by the European Academy of Wind Energy, Wind Energy Science, 1, 1–39, https://doi.org/10.5194/wes-1-1-2016, 2016.

Veers, P., Dykes, K., Lantz, E., Barth, S., Bottasso, C. L., Carlson, O., Clifton, A., Green, J., Green, P., Holttinen, H., Laird, D., Lehtomäki, V., Lundquist, J. K., Manwell, J., Marquis, M., Meneveau, C., Moriarty, P., Munduate, X., Muskulus, M., Naughton, J., Pao, L., Paquette, J., Peinke, J., Robertson, A., Sanz Rodrigo, J., Sempreviva, A. M., Smith, J. C., Tuohy, A., and Wiser, R.: Grand challenges in the science of wind energy, Science, https://doi.org/10.1126/science.aau2027, 2019.

Wildmann, N., Rau, G. A., and Bange, J.: Observations of the Early Morning Boundary-Layer Transition with Small Remotely-Piloted Aircraft, Boundary-Layer Meteorology, 157, 345–373, https://doi.org/10.1007/s10546-015-0059-z, 2015.

Wildmann, N., Vasiljevic, N., and Gerz, T.: Wind turbine wake measurements with automatically adjusting scanning trajectories in a multi-Doppler lidar setup, Atmospheric Measurement Techniques, 11, 3801–3814, https://doi.org/10.5194/amt-11-3801-2018, 2018.

Wildmann, N., Bodini, N., Lundquist, J. K., Bariteau, L., and Wagner, J.: Estimation of turbulence parameters from scanning lidars and in-situ instrumentation in the Perdigão 2017 campaign, Atmospheric Measurement Techniques Discussions, 2019, 1–33, https://doi.org/10.5194/amt-2019-171, 2019.